Physics – Uspekhi **52** (5) 461 – 486 (2009)

REVIEWS OF TOPICAL PROBLEMS PACS numbers: **32.80.–t**, **36.40.–c**, 41.60.Cr, 42.55.Vc, 42.62.Fi, **52.50.–b**, 82.50.Hp

The spectroscopy of clusters by intense pulses of VUV radiation from free electron lasers

G N Makarov

DOI: 10.3367/UFNe.0179.200905b.0487

Contents

Abstract. **High-power free electron lasers (FELs), recently developed sources for producing intense femtosecond pulses of vacuum ultraviolet (VUV) radiation, offer new ways of studying the interaction of radiation with matter. In this paper, a first series of experiments on the laser excitation of atomic cluster beams is reviewed, which showed that intense VUV pulses interact with clusters very differently than their optical or near infrared (IR) counterparts do. The first experimental results on cluster beam spectroscopy performed with intense VUV-FEL pulses are examined. FEL operation principles and performance parameters are briefly discussed. How intense ultrashort IR and VUV pulses excite clusters is analyzed, the interaction parameters between radiation and clusters are covered, and the formation and heating mechanisms of cluster plasma are explored. What is similar and fundamentally different between the ways IR and VUV radiations excite clusters is pointed out. Some other applications of VUV and soft X-ray FEL radiation are reviewed as well.**

G N Makarov Institute of Spectroscopy, Russian Academy of Sciences, 142190 Troitsk, Moscow region, Russian Federation
Tel. (7-496) 751 02 32
Fax (7-496) 751 08 86
E-mail: gmakarov@isan.troitsk.ru

Received 16 May 2008, revised 18 July 2008
Uspekhi Fizicheskikh Nauk **179** (5) 487 – 516 (2009)
DOI: 10.3367/UFNr.0179.200905b.0487
Translated by Yu V Morozov; edited by A Radzig

1. Introduction

The processes of interaction between intense femtosecond laser pulses and atomic cluster beams have been the focus of attention for the past 10 – 15 years (see, for instance, papers [1 – 18] and references cited therein). The main objective of these works, besides studying the basic aspects of matter–radiation interaction, is the production of photons or particles of much greater energy than the quantum energy of an exciting laser pulse, i.e., the generation of higher harmonics and X-ray radiation, high-energy ions, electrons, and neutrons. The structure of a cluster beam is intermediate between that of gaseous and solid-state targets. The density of atoms in clusters being almost as high as in solids, it enables a great specific energy to be deposited into them (commensurate with that for solid targets, as opposed to gaseous ones). On the other hand, the relatively small size and isolation of clusters in a beam prevent rapid relaxation (or transfer) of the energy deposited to them; hence the possibility of achieving a high degree of cluster excitation. A highly ionized cluster plasma resulting from cluster excitation by intense ultrashort laser pulses constitutes an efficacious source of X-ray radiation [19 – 31] and neutrons [32 – 42].

The characteristic size of clusters in a beam in such experiments normally varies from 5 to 100 nm, and the number of atoms in a cluster is $N \approx 10^3 - 10^7$. Clusters excited by intense laser pulses turn into completely ionized plasma that is at first located within the space occupied by the clusters but thereafter expands into its surroundings under the action of Coulomb and/or hydrodynamic forces. The length of the exciting pulse must be smaller than the plasma expansion time if cluster matter is to be excited. It is only in

this case that the whole laser pulse interacts with a not yet decomposed cluster. For a cluster characteristic size of around 10 nm ($N \approx 10^4$) and an ion expansion rate of $10^7 - 10^8$ cm s^{-1}, the ion expansion time ranges $10^{-13} - 10^{-12}$ s. This explains why effective cluster excitation, and the creation and strong heating of cluster plasma are feasible only with the use of intense femtosecond laser pulses. Notice that matter expansion time for a cluster strongly depends on the mass of its constituent atoms (see Section 2.1). For example, the initial radius (5 nm) of a deuterium cluster doubles at an electron temperature of 1 keV for only 20 fs [1], compared with 300 fs for a xenon cluster radius.

The overwhelming majority of experiments on cluster excitation by intense femtosecond pulses have been performed using near-IR lasers (Ti-sapphire lasers with a radiation wavelength $\lambda \approx 800$ nm; see reviews [1 – 11]). Only a few experiments were done using ultraviolet (UV) laser pulses (see, e.g., Refs [19, 43, 44]). A characteristic feature of cluster interaction with IR and optical pulses is that the laser radiation frequency is much lower than that of atomic transitions. At the same time, the radiation wavelength is significantly higher than the cluster size, meaning that all atoms within a cluster are in equal conditions with respect to exciting pulse intensity. These peculiarities to a large extent determine both the interaction of IR laser pulses with clusters and the further evolution of cluster plasma (see Sections 2 and 3).

Sources of intense femtosecond pulses of VUV radiation ($\lambda \leqslant 100$ nm) have recently become available. These are high-power free electron lasers built around large linear particle accelerators and characterized by high gains. To date, two large-scale VUV and soft X-ray FEL projects are underway, one in Stanford (USA) [45, 46] and the other near Hamburg (Germany) [47 – 49]. The German experiment has already yielded radiation in the far-UV and soft X-ray spectral regions [50 – 53]. Lasers emitting VUV and soft X-ray radiation have good prospects and open up new possibilities for the study of interactions between matter and radiation. They are likely to find wide application in many scientific disciplines, such as physics, chemistry, biology, and materials science. The first experiments with the employment of these lasers to excite atomic cluster beams have recently been conducted. The frequency of VUV-FEL radiation, unlike that of IR pulses, is comparable with the characteristic atomic frequency. This fact is crucial in the context of interactions between laser radiation and cluster beams (see Sections 2 and 5). The data obtained illustrate interaction patterns of VUV pulses and clusters differing from IR radiation–cluster interactions.

This review presents the results of early experiments on atomic cluster beam spectroscopy using intense pulses of VUV-FEL radiation. The constituent elements, principles of operation, and characteristics of FELs are briefly discussed, along with radiation pulse properties. The parameters of atomic cluster interaction with IR and VUV pulses are considered. Processes of cluster excitation by intense ultrashort IR and VUV radiation pulses are subjected to analysis. Cluster plasma ionization and heating mechanisms in these two cases are examined. General concepts of cluster excitation by IR and UV radiation pulses are formulated and fundamental differences between the two processes are emphasized. Some other applications of VUV and soft X-ray FEL radiation are exemplified.

The review outline is as follows. Section 2 deals with the qualitative picture of cluster dynamics under the effect of laser pulses and most important parameters of cluster–radiation interaction. Cluster excitation by intense IR pulses is briefly considered in Section 3 to compare its results with those of VUV pulse excitation and to obtain a deeper insight into similar and different processes. Mechanisms of cluster ionization, formation, and the strong heating of cluster plasma under excitation by IR pulses are analyzed. Section 4 focuses on the VUV free electron lasers. It briefly describes the construction and principles of operation of the laser as well as main properties of radiation pulses. Prospects for the application of such lasers in some related scientific disciplines are highlighted. Section 5, which is central to this review, is devoted to cluster spectroscopy using intense pulses of VUV-FEL radiation. The results of the first experiments designed to excite xenon cluster beams by VUV radiation of FELs are presented, and models for their explanation are developed. Experimental and simulation work on photoelectron and photoion spectroscopy of argon and xenon cluster beams is analyzed. The mechanisms of cluster ionization, strong heating of cluster plasma, and absorption of a large number of photons by the clusters from the laser pulse field are examined. Cluster excitation by intense IR pulses is compared with that by VUV radiation pulses. Some other examples of FEL applications are given, e.g., in two-frequency (excitation–probing) experiments and for the ablation of materials. The concluding section summarizes the results of research and provides their relevant interpretation.

2. The qualitative picture of cluster dynamics under the effect of laser pulses and selected parameters of cluster-radiation interaction

2.1 Cluster dynamics under the effect of a laser pulse

It seems appropriate that consideration of cluster excitation by intense IR and VUV laser pulses be preceded by a concise analysis of a qualitative picture of cluster dynamics under the action of laser pulses and some important parameters of cluster–radiation interaction. A cluster affected by a laser pulse undergoes the following processes [1 – 11]: (1) internal ionization of cluster atoms, giving rise to quasi-free electrons and nanoplasma; (2) heating of the quasi-free electrons inside the cluster; (3) external cluster ionization due to electron emission from the highly ionized cluster, and (4) complete fragmentation of the cluster resulting from a Coulomb and/or hydrodynamic explosion. These processes occur in all clusters exposed to intense laser pulses regardless of the radiation wavelength. Some of these processes (e.g., 1 and 2, 1 and 3, 2 and 3) may coincide in time.

In other words, interactions between a laser pulse and clusters lead to their conversion into a system of multiply charged ions and free electrons [1, 3, 4, 8, 9]. Part of the electrons leave the cluster that acquires a positive charge, while the other part is retained by the cluster's self-consistent field. The resulting system of multicharge ions and electrons is unstable and decays owing to ion spreading out. Characteristic decay time $\tau_{\rm exp}$ is given by [1, 18]

$$\tau_{\rm exp} \sim R_0 \left(\frac{m_{\rm i}}{Z' k T_{\rm e}} \right)^{1/2} \left(\frac{n_0}{n_{\rm e}} \right)^{1/3}, \qquad (2.1)$$

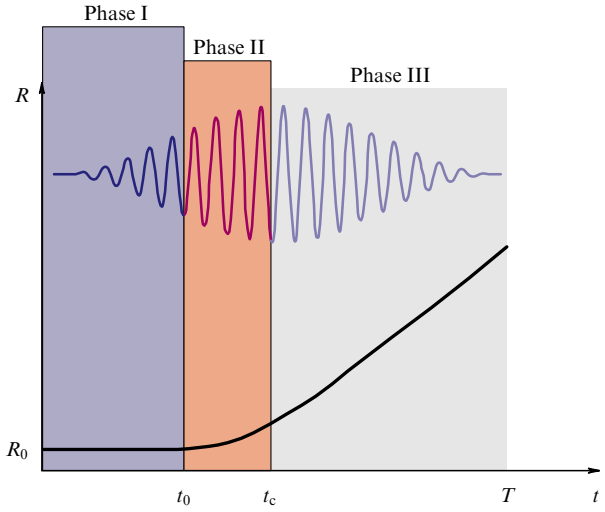

Figure 1. Qualitative picture of cluster dynamics under the effect of an intense laser pulse: $R(t)$ — time-dependent cluster radius. The figure shows atomic ionization (phase I), the critical expansion phase (phase II), and relaxation (phase III), as well as the exciting laser pulse; T — total time of the three-stage cluster evolution [8].

where R_0 is the initial cluster radius, Z' is the charge of the cluster ion, T_e is the cluster's electron temperature, m_i is the ion mass, n_0 and n_e are the initial and running electron concentrations, and k is the Boltzmann constant. Notice that the running electron concentration n_e is strongly time-dependent; this dependence needs to be taken into consideration when estimating cluster expansion time. As the system breaks down with an ion velocity, its decay time may be considerably greater than the duration of the laser pulse. This stage of development of the evolving plasma may affect its properties [1–4, 8, 9]. The interaction being considered between the cluster beam and the intense short IR laser pulse makes it possible to deposit a high specific energy (1–10 keV per electron) into the electron subsystem. In this way, absorption of laser pulse energy by the cluster beam leads to the formation of a specific hot plasma [1, 3, 4, 8, 9].

Cluster evolution in time may be described as a three-stage process (Fig. 1) [8]. At the first stage (phase I), the laser pulse interacts with cluster atoms as if they were isolated. The laser field produces primary single internal ionization of neutral cluster atoms. Multiply charged atomic ions prevailing in the cluster are produced due to collisions of hot electrons with atoms and ions and due to atomic ionization by the Coulomb field of the charged cluster after it is left by part of its electrons ('ignition mechanism'; see Sections 3.5 and 5.1). These processes lead to atomic ionization within the cluster and formation of quasi-free electrons inside the cluster. At the most important and interesting stage, phase II, the cluster expands under the action of Coulomb forces of the newly formed ions. Expansion of the cluster results in decreased ion density. On the other hand, the density of quasi-free electrons in the cluster can be unaltered. These electrons formed by virtue of internal cluster ionization (see Section 3) remain coupled with the cluster as a whole rather than with individual ions. Their density changes depending on the balance between internal and external cluster ionization rates at a given instant of time. Finally, energy absorption from the laser pulse decreases at stage III as the pulse becomes weaker and then ceases. Energy redistribution within the cluster occurs during this stage, e.g., by recombination, until it undergoes complete fragmentation and energy distributions of electrons and ions are established. This simplified but rather universal scheme permits us to better understand and define various mechanisms of energy absorption by the cluster. In the case of a short exciting laser pulse, the processes of cluster expansion and the establishment of equilibrium occur after the pulse cessation.

2.2 Selected parameters of cluster-radiation interaction

Figure 1 also schematically depicts an exciting laser pulse. When the length of an IR pulse is close to 100 fs, the number of its field strength oscillations ($\lambda = 800$ nm, $\omega = 2\pi c/\lambda \cong 2.4 \times 10^{15}$ s^{-1}) is approximately 37, compared with some 300 in a VUV pulse ($\lambda = 100$ nm, $\omega \cong 2 \times 10^{16}$ s^{-1}). As already indicated in Section 1, the laser field frequency ω in IR pulses is significantly smaller than the atomic frequency ω_a:

$$\omega \ll \omega_a = \frac{m_e e^4}{\hbar^3}\,, \tag{2.2}$$

where m_e and e are the electron mass and charge, respectively, and $\hbar$ is Planck's constant. In the case of VUV pulses, the laser frequency can exceed the atomic frequency. Atomic frequency given by relation (2.2) is $\omega_a \cong 4.13 \times 10^{16}$ s^{-1}, and the corresponding atomic wavelength $\lambda_a \cong 45.6$ nm. This means that the radiation wavelength during cluster excitation by VUV pulses can be smaller than or similar to the atomic wavelength. In contrast, the radiation wavelength in the case of excitation by IR pulses is much greater than the atomic wavelength. All these differences explain why cluster excitation by VUV pulses is so dissimilar from IR pulse excitation (see Sections 3 and 5).

Knowledge of the limits of applicability of the perturbation theory is necessary to describe cluster excitation by intense IR and VUV laser pulses. The perturbation theory does not work when radiation intensity exceeds a critical value I^* given by the relation [8]

$$I^* \sim F^2 \sim 4\omega^2 \Delta E\,, \tag{2.3}$$

where ΔE is the typical difference between atomic energy levels (e.g., ionization potential), F is the strength of the laser pulse electric field, and ω is the radiation frequency. Notice the quadratic frequency dependence of I^*. It makes the perturbation theory applicable in the case of cluster excitation by VUV pulses, even at a high intensity of the laser field, as illustrated by Table 1 containing the intensities given by relation (2.3) for different laser frequencies at $\Delta E = 1$ Ry (≈ 13.6 eV).

A relation analogous to Eqn (2.3) is possible to derive evaluating the laser field intensity at which electrons tunnel across the potential barrier created by the joint action of an ion field and the laser field during a time smaller than the length of the laser pulse. This intensity is determined by the

Table 1. Laser radiation intensities I^* representing the boundary values for the process of cluster ionization in the framework of perturbation theory and exact solution in accordance with relationship (2.3) for different wavelengths and radiation frequencies [8].

λ, nm	780	100	3.5
$\hbar\omega$, eV	1.59	12.4	350
I^*, W cm^{-2}	5×10^{14}	3×10^{16}	2×10^{19}

Keldysh parameter $\gamma = T_1\omega$, where T_1 is the tunneling time [54]. The Keldysh parameter can be rewritten in the form [8]

$$\gamma = \sqrt{\frac{\Delta E}{2E_{\mathrm{p}}}}. \tag{2.4}$$

Here, E_{p} is the ponderomotive energy ('quiver' or vibrational energy) of an electron in the oscillating laser field, defined as

$$E_{\mathrm{p}} = \frac{e^2F^2}{4m_{\mathrm{e}}\omega^2}. \tag{2.5}$$

The value of $\gamma = 1$ sets an approximate borderline between the regimes in which the perturbation theory works, $\gamma \gg 1$ (multiphoton excitation of atoms), and when it does not, $\gamma \leqslant 1$. The strength of the oscillating laser field is especially important for relatively extended systems, such as clusters. It determines the quiver amplitude of electrons, x_{quiv}, i.e., the amplitude of periodic electron motion under the action of the laser field:

$$x_{\mathrm{quiv}} = \frac{eF}{m_{\mathrm{e}}\omega^2}. \tag{2.6}$$

This amplitude is usually compared with a cluster radius measuring about 50 Å for Xe_N clusters with the number of atoms $N = 10^4$. Table 2 includes Keldysh parameters as well as absolute values of ponderomotive energy E_{p} and electron oscillation amplitudes x_{quiv} for some laser wavelengths considered in this review at different intensities. These parameters and quantities characterize radiation–cluster interactions and can be used to analyze different mechanisms of cluster ionization and heating of cluster plasma (see Sections 3 and 5).

To close this section, is should be noted that the dipole approximation remains valid, short wavelengths of exciting radiation from an FEL in the VUV range notwithstanding. This inference follows from the comparison of electron oscillation amplitudes with radiation wavelengths (see Table 2). The latter quantity is several orders of magnitude greater than the former, even at high intensities. Moreover, interactions between laser pulses and an atomic system have a non-relativistic nature despite the large wave amplitude of the exciting radiation [9]. Indeed, the characteristic velocity of valence electrons in an atom is roughly $e^2/\hbar$. For atomic ions with charge $Z \sim 1$, it is of the same order: $v \sim Ze^2/\hbar$; therefore, the parameter v/c, where c is the speed of light in vacuum, is small. It accounts for the nonrelativistic character of interactions between the atoms and ions under consideration with the electromagnetic field.

Table 2. Keldysh parameter γ, 'quiver' amplitude of electrons x_{quiv}, and ponderomotive energy E_{p} for long- and short-wave laser radiation at different intensities [8].

	Intensity, W cm^{-2}			
Wavelength, nm		10^{14}	10^{16}	10^{18}
780	γ E_{p}, eV x_{quiv}, Å	1.55 5.67 8.28	0.15 567 82.8	0.015 56.7×10^3 828
100	γ E_{p}, eV x_{quiv}, Å	12.1 93×10^{-3} 0.136	1.21 9.3 1.36	0.121 932 13.6
3.5	γ E_{p}, eV x_{quiv}, Å	345 1×10^{-4} 0.0002	34.5 0.01 0.002	3.45 1.1 0.02

3. Cluster excitation by intense IR pulses

3.1 General remarks

The cluster excitation by ultrashort laser pulses in the IR range ($\lambda \approx 800$ nm) has been the subject of many studies (see, for instance, papers [1–4, 8, 9] and references cited therein). Typical energy fluxes of laser light in such experiments are $10^{14}-10^{20}$ W cm^{-2}, and the pulse length τ_{p} falls in the range 30 to 300 fs. The strength of the electric field in a laser wave at high radiation intensities is much greater than the characteristic field strength in a hydrogen atom. For example, a characteristic atomic value for the electric field strength amounts to

$$F_{\mathrm{a}} = \frac{e}{a_0^2} = \frac{m_{\mathrm{e}}^2e^5}{\hbar^4} \cong 5.14\times10^9 \text{ V cm}^{-1}, \tag{3.1}$$

while the corresponding intensity of the electromagnetic wave is estimated as

$$I = \frac{cF_{\mathrm{a}}^2}{8\pi} \cong 3.5\times10^{16} \text{ W cm}^{-2}. \tag{3.2}$$

Here, e is the electron charge, a_0 is the Bohr radius, m_{e} is the electron mass, $\hbar$ is Planck's constant, and c is the speed of light. Pulse fields created by modern lasers may be several orders of magnitude stronger; due to this, a laser pulse can ionize cluster atoms as the result of an above-barrier transition of electrons. Moreover, the same applies to the ions being produced. Fast excitation of a cluster in the absence of a heat removal mechanism leads to the strong heating of the cluster's electron subsystem (up to 1–10 keV). In this case, atomic ions are practically unheated at the onset of laser pulse action. After fast initial multiple ionization, during the larger part of a laser pulse cluster ions constitute an ideal plasma comprising electrons and multiply charged atomic ions. A number of processes occur in a strongly excited cluster during its excitation by a laser pulse and after the pulse cessation [1–11]. The cluster undergoes both internal and external photoionization, Coulomb and hydrodynamic explosions with the concurrent generation of higher harmonics and X-ray radiation, nuclear fusion, and neutron production.

3.2 Mechanisms of atomic ionization

The process of interaction between intense IR laser pulses and cluster atoms is substantially different from interactions of intense pulses with atoms in the gaseous phase even though the primary mechanism of atomic ionization and plasma formation is common to both cases (tunnel or above-barrier ionization of atoms). However, subsequent processes of plasma ionization and heating are different. The atomic number density in a gas being small, collisions between electrons and ions over the time scale of a laser pulse are rare. For this reason, the predominant mechanism of plasma formation is direct optical ionization of the atoms by the laser field. At radiation intensities used in such experiments ($10^{14}-10^{20}$ W cm^{-2}), the first electrons arise from tunnel (or above-barrier) ionization of the atoms [55].

There are three primary heating mechanisms operating in a plasma produced by tunnel ionization of atoms in a gas. One (above-threshold ionization, ATI) is the single atom effect. It is realized through the absorption of additional energy from the laser field during ionization; for a linearly polarized field, this energy is estimated as follows [1]:

$$E_{\mathrm{ATI}} = 2U_{\mathrm{p}} \sin \Delta\varphi \,. \tag{3.3}$$

Here, U_{p} is the ponderomotive potential at the instant of time when atoms undergo ionization, which is given [1] by the expression U_{p} (eV) $= 9.3 \times 10^{-14}\ I(\mathrm{W\ cm^{-2}}) \times \lambda^2$ (μm), and $\Delta\varphi$ is the phase counted off from the peak magnitude of the laser electric field at which an atom is ionized. The maximum energy of electrons in such a model amounts to $2U_{\mathrm{p}}$. By way of example, in the case of helium atom ionization (with radiation parameters $\lambda = 800$ nm, $\tau_{\mathrm{p}} = 100$ fs, $I = 10^{17}$ W cm^{-2}), one obtains $E_{\mathrm{ATI}} > 100$ eV. However, the peak of electron energy distribution falls on the zero energies. Owing to this, the distribution 'temperature' [defined as $kT_{\mathrm{e}} = (2/3)\langle E \rangle$] is rather low (around 40 eV). Results of calculations [55] and experimental findings [56] indicate that, in the general case, the plasma temperature during ATI does not exceed 50 eV for the gases He, Ar, or Kr under excitation by radiation pulses with a wavelength of 800 nm, duration of 100 fs, and intensity of 10^{17} W cm^{-2}.

Another electron heating mechanism is attributed to elastic Coulomb collisions of ions with electrons moving under the action of a laser field in a gas [inverse bremsstrahlung (IBS)]. For typical gas densities, this mechanism is less important than the ATI mechanism [57]. The energy deposition rate per electron may be written as

$$\frac{\partial E_{\mathrm{col}}}{\partial t} = 2\nu_{\mathrm{ei}} U_{\mathrm{p}} \,, \tag{3.4}$$

where ν_{ei} is the frequency of electron–ion collisions (normally sought in the strong and weak field limits [1, 3, 4]). In the strong field limit, it appears [1] that the plasma heating rate is about 3 eV ps^{-1} for an He plasma with a temperature of 10 eV and ion number density of 10^{18} cm^{-3} at an intensity of 10^{16} W cm^{-2}. This means that the contribution of this mechanism to gas plasma heating in the general case for subpicosecond laser pulses is insignificant.

The third plausible mechanism of gas plasma heating is governed by simulated Raman scattering (SRS) [58]. However, it was shown in Refs [59, 60] (see also paper [1]) that this mechanism proves to be important only at IR radiation intensities above 10^{18} W cm^{-2}, and less so at lower intensities. In other words, temperatures of low-density gases of interest exposed to IR laser pulses some 100 fs in length at intensities below 10^{17} W cm^{-2} usually lie in the range from 10 to 50 eV. Much higher temperatures are achieved for clusters where atomic number density is high and the number of electron–electron and electron–ion collisions is great. Mechanisms of cluster plasma ionization and heating are briefly considered in Sections 3.3, 3.4, and 3.5 below.

3.3 Mechanisms of internal cluster ionization

Mechanisms of internal and external cluster ionization are many [1, 3, 4, 8, 9]. We shall briefly consider only the best known ones. Attention is usually focused on three mechanisms of internal ionization [1], playing the key role during interactions between laser radiation and cluster atoms. The first is direct optical (tunnel or above-barrier) ionization of atoms. It is of special importance at the early stages of laser pulse–cluster interaction because it gives rise to the initial electrons that form the plasma. The tunnel ionization rate may be calculated from the atomic ionization rate averaged over the laser field cycle, which was devised in the classical work by Ammosov, Delone, and Krainov [55]. This rate for an arbitrary atom is given by the expression

$$W_{\mathrm{tun}} = \omega_{\mathrm{a}} \frac{(2l+1)(l+|m|)!}{2^{|m|}|m|!(l+|m|)!} \left(\frac{2e}{n^*}\right)^{n^*} \frac{1}{2\pi n^*} \times I_{\mathrm{p}} \left(\frac{2F}{\pi (2I_{\mathrm{p}})^{3/2}}\right)^{1/2} \left(\frac{2(2I_{\mathrm{p}})^{3/2}}{F}\right)^{2n^*-|m|-1} \times \exp\left[-\frac{2(2I_{\mathrm{p}})^{3/2}}{3F}\right] . \tag{3.5}$$

Here, l and m is the quantum numbers of angular momenta (the rate is averaged over m for the electron shell), ω_{a} is the atomic frequency ($\omega_{\mathrm{a}} \cong 4.13 \times 10^{16}$ s^{-1}), n^* is the effective principal quantum number, $n^* = Z\,[2I_{\mathrm{p}}(\mathrm{eV})]^{-1/2}$, Z is the ion charge, F is the laser field strength in Hartree atomic units, and I_{p} is the ionization potential in atomic units. The rate in question is a strongly nonlinear one with respect to the laser field. Laser radiation intensities of roughly 10^{14} W cm^{-2} are usually needed to ensure efficacious tunnel ionization of atoms in the event of subpicosecond pulses. For example, 100% ionization of Ar atoms under the effect of a 100-fs pulse occurs when the peak radiation intensity amounts to $\sim 3 \times 10^{14}$ W cm^{-2} [1].

The above-barrier ionization can be described [3, 9] in the framework of the Bethe approximation [61]. Assuming that the released electron spends time in the Coulomb field of the atomic core and the laser field does not change the ionization potential of the atomic particle, the electric potential acting on the electron has the form (in atomic units)

$$U = -\frac{Z}{r} + Fx \,, \tag{3.6}$$

where r is the distance between the electron and the atomic core, x is the coordinate along the field, Z is the atomic core charge, and F is the actual wave field strength. The above-barrier release of electrons takes place when the field strength complies with relation [3, 61]

$$F > \frac{I_{\mathrm{p}}^2}{4Z} \,, \tag{3.7}$$

where I_{p} is the ionization potential of an atomic particle. Using the ionization potential of a hydrogen-like ion $I_{\mathrm{p}} = Z^2 I_0/n^2$ (I_0 is the ionization potential of a hydrogen atom in the ground state, and n is the principal quantum number; the relation holds for large Z) brings about the following equation for the maximum charge of an atomic ion produced by a field of strength F:

$$Z = n^{4/3} \left(\frac{F}{F_{\mathrm{a}}}\right)^{1/3} , \tag{3.8}$$

where the parameter F_{a} is given by formula (3.1). Relationship (3.8) makes it possible to evaluate the field strength dependence of the ion charge [3, 9].

The second mechanism of cluster ionization is probably the most important one in the case of cluster excitation by near-IR pulses. It is attributed to ionization due to inelastic electron–ion collisions within a cluster. As soon as optical ionization yields primary electrons, the majority of ions in

high-charge states appear as a result of collisional ionization owing to high particle number density in the cluster. The rate of collisional ionization is usually computed [1, 3, 7] from the Lotz empirical formula [62]. The rate per ion averaged over Maxwellian electron velocity distribution is defined by the expression

$$W_{kT} = n_{\mathrm{e}} \frac{a_{\mathrm{i}} q_{\mathrm{i}}}{I_{\mathrm{p}} (kT_{\mathrm{e}})^{1/2}} \int_{I_{\mathrm{p}}/kT_{\mathrm{e}}}^{\infty} \frac{\exp(-x)}{x} \, \mathrm{d}x \,, \tag{3.9}$$

where n_{e} is the electron number density, I_{p} is the ionization potential (in electron-volts), a_{i} is an empirical constant equaling 4.5×10^{-14} eV^2 cm^{-3} [62], and q_{i} is the number of electrons in the outer ion shell. Electron energy must satisfy the inequality $kT_{\mathrm{e}} \geqslant I_{\mathrm{p}}$. For conditions realized in a cluster, this rate may be rather high. By way of example, the rate of argon atom ionization from Ar^{8+} to Ar^{9+} ($I_{\mathrm{p}} = 422$ eV) reaches 0.3 fs^{-1} in an argon cluster with solid-state density and octuply ionized atoms ($Z = 8$, $n_{\mathrm{e}} = 2 \times 10^{23}$ cm^{-3}) at a temperature of 1 keV. Therefore, this ionization mechanism may be responsible for the formation of high-charge-state ions at intensities much below the threshold ones necessary for cluster tunnel ionization, provided the clusters are sufficiently hot. Observe that tunnel ionization of Ar^{8+} to Ar^{9+} acquires significance only at intensities above 10^{18} W cm^{-2} [1].

The third mechanism covers collisional ionization of cluster atoms by electrons oscillating in the laser field. Expression (3.9) takes account only of the collisional ionization rate due to the electrons' thermal energy. Electrons in a cluster also acquire the velocity component related to their oscillating movements in the laser field. In the general case, calculation of the ionization rate due to electron oscillations is a difficult task posed by the large number of Coulomb collisions encountered by electrons that interfere with their sinusoidal movements. Nonetheless, the rate of ionization attributable to this mechanism can be estimated from above regarding electron velocity as purely sinusoidal. Such an estimation was undertaken in Ref. [1]. The authors used the expression for the collisional ionization cross section depending on the particle velocity, which was proposed in Ref. [62]:

$$\sigma_{\mathrm{i}} = a_{\mathrm{i}} q_{\mathrm{i}} \frac{\ln(E_{\mathrm{e}}/I_{\mathrm{p}})}{E_{\mathrm{e}} I_{\mathrm{p}}} \,, \tag{3.10}$$

where E_{e} is the electron kinetic energy, and I_{p} is the ionization potential of the atoms. The ionization rate per ion is defined as follows:

$$W_{\mathrm{las}}(t) = n_{\mathrm{e}} \sigma_{\mathrm{i}} \frac{eF_{\mathrm{in}}}{m_{\mathrm{e}} \omega} \, |\sin \omega t| \,, \tag{3.11}$$

where F_{in} is the intracluster electric field [see relation (3.14)].

The collisional ionization rate per ion averaged over the laser field period is given by [1]

$$W_{\mathrm{las}} \approx n_{\mathrm{e}} \frac{a_{\mathrm{i}} q_{\mathrm{i}}}{2\pi I_{\mathrm{p}} m_{\mathrm{e}}^{1/2} U_{\mathrm{p}}^{1/2}} \times \left\{ \left[3 + \frac{I_{\mathrm{p}}}{U_{\mathrm{p}}} + \frac{3}{32} \left(\frac{I_{\mathrm{p}}}{U_{\mathrm{p}}} \right)^2 \right] \ln \left[\frac{1 + \sqrt{1 - I_{\mathrm{p}}/2U_{\mathrm{p}}}}{1 - \sqrt{1 - I_{\mathrm{p}}/2U_{\mathrm{p}}}} \right] - \left(\frac{7}{2} + \frac{3I_{\mathrm{p}}}{8U_{\mathrm{p}}} \right) \sqrt{1 - \frac{I_{\mathrm{p}}}{2U_{\mathrm{p}}}} \right\} . \tag{3.12}$$

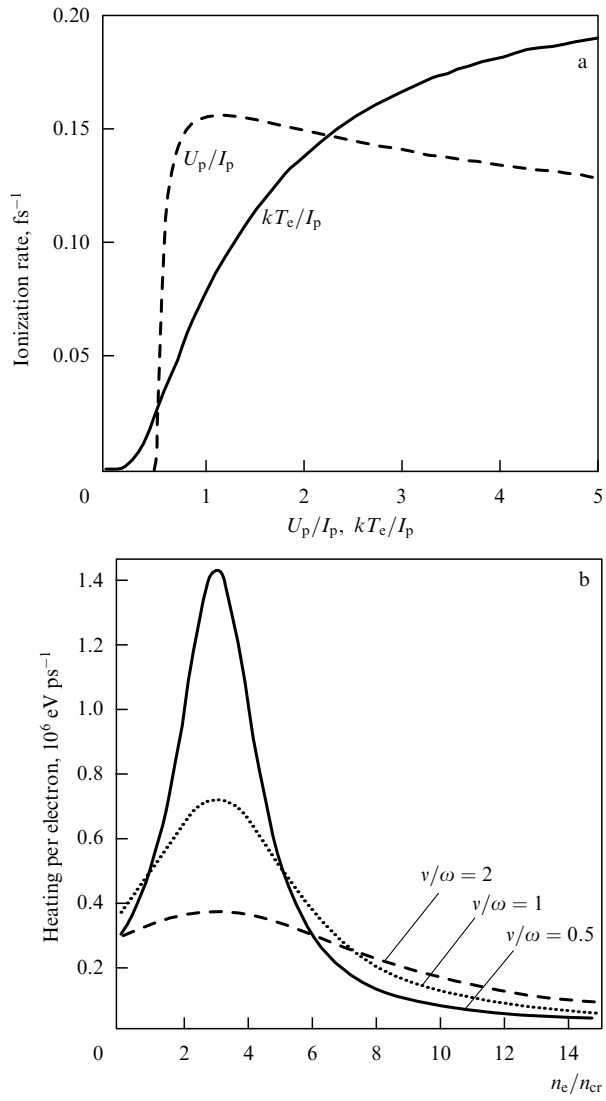

Figure 2. (a) Calculated rate of Ar^{8+} ion ionization in a plasma with an electron number density of 10^{23} cm^{-3} by thermally heated electrons (solid line) and electrons set in motion by the laser field (dashed line) [1]. (b) Calculated rate of cluster heating by a laser pulse with a wavelength of 825 nm and intensity of 10^{16} W cm^{-2}, derived from relation (3.17) depending on electron concentration for three collision frequencies [1].

Notice that simpler expressions for the collisional ionization rate of atoms inside a cluster at different U_{p}-to-I_{p} ratios were derived in Refs [3, 4, 7]. Figure 2a depicts the ionization rate for Ar^{8+} ions as a function of $U_{\mathrm{p}}/I_{\mathrm{p}}$ at an electron number density of 1×10^{23} cm^{-3}. This rate is compared with the thermal ionization rate defined by relation (3.9) as a function of $kT_{\mathrm{e}}/I_{\mathrm{p}}$. As follows from Fig. 2a, these two quantities are commensurable if the plasma temperature is comparable to the ponderomotive energy of the laser field inside the cluster.

3.4 Cluster heating mechanisms

Because the cluster thermal ionization rate is essentially dependent on the electron temperature, it is important to obtain an insight into the cluster heating mechanism. One of the first studies addressing cluster ionization dynamics and heating upon exposition to intense laser pulses was reported in Ref. [1] and contained phenomenological consideration of a cluster nanoplasma model. The authors analyzed interac-

tions of a laser pulse with a cluster regarded as a small sphere of high-density plasma. The number density of quasi-free electrons inside the cluster, $n_e(t)$, was assumed to be spatially uniform but time-dependent. Time dependence of electron density permits taking into account laser pulse-induced dynamics. The assumption of plasma homogeneity requires that the cluster size be significantly greater than the Debye shielding length

$$\lambda_D = \sqrt{\frac{kT_e}{4\pi e^2 n_e}}. \tag{3.13}$$

This quantity imposes limitations on the spatial size of a plasma with electron temperature T_e. For example, one finds $\lambda_D \sim 5$ Å at $kT_e = 1000$ eV for a plasma with a density of 10^{23} cm^{-3}, typical of a solid. This means that the nanoplasma model describes only clusters with radius $R \gg 5$ Å. Notice that the concentration of electrons in a cluster at $kT_e \approx 1$ keV exceeds 10^{23} cm^{-3} due to multiple atomic ionization. Electron concentration increases with a further rise in temperature; owing to this, the Debye length λ_D always remains very small compared with the size of the clusters considered in this review.

Temporal evolution of electron density in the model under consideration is evaluated in the self-consistent way — that is, electric field F_{in} inside the cluster depends [via dielectric constant $\varepsilon(\omega)$] on electron density $n_e(t)$, while density variations $n_e(t)$ are controlled through the ionization of atoms and ions by the electric field F_{in}. The cluster diameter in the case of interest being much smaller than the laser wavelength, it can be assumed that the field in the cluster equals the field inside the dielectric sphere placed in a constant electric field. This field is given by the expression [63]

$$F_{in} = \frac{3}{|2 + \varepsilon(\omega)|} F, \tag{3.14}$$

where F is the electric field strength in a vacuum, and dielectric constant is usually taken in the Drude form [64]:

$$\varepsilon(\omega) = 1 - \frac{\omega_p^2}{\omega(\omega + i\nu_{ei})}, \tag{3.15}$$

where $\omega_p = \sqrt{4\pi e^2 n_e/m_e}$ is the plasma frequency, and ν_{ei} is the electron–ion collision frequency.

Because the cluster is assumed to have no temperature gradients, laser heating should be uniform throughout its bulk. Also, it is supposed that the energy of laser excitation is initially deposited into free electrons inside the cluster by virtue of inverse bremsstrahlung. The electron heating rate can be deduced from the rate of energy deposition into the dielectric sphere. The heating rate averaged over the laser field cycle is defined as [1]

$$\frac{dE_e}{dt} = \frac{\omega}{8\pi} \operatorname{Im}[\varepsilon] |F_{in}|^2. \tag{3.16}$$

With relations (3.14) and (3.15) taken into account, the heating rate per unit volume assumes the form [1]

$$\frac{dE_e}{dt} = \frac{9\omega^2\omega_p^2\nu}{8\pi} \frac{1}{9\omega^2(\omega^2+\nu^2)+\omega_p^2(\omega_p^2-6\omega^2)} |F|^2. \tag{3.17}$$

An important fact is that when electron density within a cluster sphere is high, i.e., when $n_e/n_{e,cr} \gg 3$ (where critical electron density $n_{e,cr} = m_e\omega^2/4\pi e^2$), then the field strength in the cluster defined by expression (3.14) is smaller than the field strength in the vacuum outside the cluster. Such laser field shielding results in a decreased rate of cluster heating. However, when $n_e/n_{e,cr} = 3$, function $|\varepsilon(\omega) + 2|$ passes through a minimum. In this case, the laser field inside the cluster strengthens as opposed to the external field, and the cluster heating accelerates [1]. The relative amplitude and width of this resonance, referred to as Mie resonance [65], depend on collision frequency ν_{ei}. The $n_e/n_{e,cr}$ dependences of heating rates described by relation (3.17) for certain fixed collision frequencies ν_{ei} are shown in Fig. 2b. It can be seen that the cluster heating rate grows with increasing electron density, reaches a maximum, and falls again below its values in a vacuum at $n_e/n_{e,cr} \geqslant 5$.

The model of cluster plasma heating proposed in Ref. [66] is based on similar ideas. However, electron density in a cluster was assumed to depend on its radius: $n_e = n_e(R, t)$. It was shown that the predominant mechanism of energy absorption is attributed to resonant absorption by electrons at the cluster surface, when the condition $n_e \sim 3n_{e,cr}$ is fulfilled. In the course of time, such resonant absorption transfers from the cluster surface layers to the bulk and lasts a rather long time (usually throughout the entire duration of the exciting laser pulse, i.e., several hundred femtoseconds) until maximum electron density in the bulk of the cluster becomes lower than the above value.

The phenomenological approach to the description of cluster excitation considered in the preceding paragraphs is based on a number of approximations that need verification. Certain later authors [67–77] considered cluster excitation in the framework of classical molecular dynamics. Modern computers make possible a microscopic description of multiparticle cluster dynamics. Many results of these works were reviewed in recent publications [8, 9], others will be discussed in Section 5.4 below. Here, we mention only the most important issues ensuing from them.

The key idea behind consideration of cluster electrons [69] that promotes a deeper understanding of physics and successful numerical simulation proceeds from resolving ionization into internal and external components (see also Refs [3, 8, 9]). Internal ionization implies excitation of bound electrons, giving rise to so-called quasi-free electrons. These electrons are not coupled to individual atoms but remain associated with a cluster ion as a whole, whose spatial charge is strong enough to retain electrons. According to the aforementioned models, such quasi-free electrons tend to spread within a cluster in a classical way among ions and other quasi-free electrons; therefore, computation takes account of all mutual Coulomb forces. For traveling electrons, consideration of their scattering from ions and other electrons is of importance by reason of high particle number density in the bulk of the cluster. Moreover, quasi-free electrons can be additionally heated by IR and VUV lasers and eventually injected into the continuum; in this way, external ionization proceeds.

IR and VUV laser pulses exciting clusters act on electrons as if they were a classical field. Quasi-free electrons affected by the oscillating laser field undergo oscillations with a sufficiently large amplitude (see Table 2) and strong heating by virtue of inverse bremsstrahlung resulting from repeating collisions of field-driven electrons with ions. In the event of

high-frequency radiation, the field oscillates so fast that the electron velocity has no time to increase appreciably. For this reason, the laser field may be disregarded in classical equations of electron motion.

Alternative mechanisms of cluster heating were also considered in Refs [78–80]. The authors of Ref. [80] arrived at the conclusion that the principal mechanism is electron heating induced by laser polarization. They expressed their opinion that the phase difference between the oscillating electron cloud of a cluster and the electron-driving laser field results in radiation absorption and cluster heating. However, it was argued somewhat later [81] that polarization interferes with dephasing and cannot be responsible for enhanced energy absorption. The authors of Ref. [81] proposed a heating mechanism underlain by backscattering of quasi-free electrons from ionic (non-Coulomb) potentials. Such backscattering is a process during which electrons transfer energy to the laser pulse electromagnetic field that is spent to further heat electrons. According to the authors of Ref. [81], this mechanism ensures an estimated tenfold rise in the yield of X-ray radiation.

Absorption of laser pulses by atomic clusters with a diameter of about 10 nm, an intensity of roughly 10^{16} W cm^{-2}, and a resonance between the cluster plasma frequency and the triple frequency of the titanium sapphire laser was investigated in Refs [82–84]. The resonance arises and disappears in the course of cluster expansion. It is found that enhanced atomic ionization proceeds at resonance, resulting in the appearance of multiply charged ions within the cluster. Simultaneously, the second harmonic of the laser pulse is also generated.

It was reported in paper [85] that part of the quasi-free electrons in a cluster absorb relatively high energy and pass through the cluster for a single laser period. Disturbance of electron harmonic oscillations at the cluster boundaries results in the enhancement of energy absorption from the laser field through inverse bremsstrahlung that may be highly efficacious. The calculations performed in Ref. [86] indicate that the efficiency of cluster heating through inverse bremsstrahlung is significantly higher (roughly by two orders of magnitude) when account is taken of electron collisions with the cluster ion as a whole rather than with individual atomic ions. Detailed analysis of cluster interactions with intense near-IR laser pulses and VUV pulses from FELs has recently been reported in Refs [80, 87, 88]. These works will be discussed in Section 5.4.

3.5 Mechanisms of external cluster ionization

Let us consider in brief mechanisms of cluster external ionization and the formation of a cluster ion. In the case of metal clusters, i.e., in the presence of conduction electrons, the primary ionization mechanism consists in the removal of these electrons from the cluster surface by the electromagnetic field of the exciting laser pulse. This mechanism is generally known as *cold* ionization [3] which ceases when the attracting force between an electron and the newly formed cluster ion exceeds the force exerted on the electron from the side of the electromagnetic field. The charge Z' of the cluster ion corresponding to the end of this process can be found from the Coulomb law:

$$Z' = FR^2 . \tag{3.18}$$

It should be noted that the number of electrons removed from a cluster during cold ionization is small compared with their total number. By way of example, in a sodium cluster of radius $R = 215$ Å and with the number of atoms $N = 10^6$, one finds $Z' = 27300$ at the field intensity 10^{15} W cm^{-2} (and the field strength 8.5×10^9 V cm^{-1}) [3], whereas the number of cluster electrons is $ZN = 1.1 \times 10^7$.

External ionization in rare gas clusters occurs due to the lowering of the electrostatic barrier of the cluster ion by the superstrong electromagnetic field of the laser pulse [3, 4, 89, 90]. Such electrons are supposed to leave both the parent atom and the cluster within the atomic time ($\sim 10^{-16}-10^{-17}$ s). It was shown in Ref. [89] that above-barrier ionization in a cluster comprising 1100 xenon atoms in a laser field of intensity 10^{16} W cm^{-2} leads to the production of a cluster ion with the charge $Z' = 1200$. Further ionization is governed by a different mechanism. The cluster ion thus formed may be treated as a conducting sphere with the charge concentrated within a thin layer at its surface. The superstrong Coulomb field in this layer knocks out additional electrons from the nearest atomic ions, which are directed toward the cluster center. These electrons pick up high speed and then leave the cluster. As a result, the charge of the cluster ion increases to $Z' = 2600$. This is the so-called *ignition* mechanism [91]. For example, the strength of the electric field at the surface of a cluster comprising 25 singly ionized neon atoms is on the order of $F = 5 \times 10^{12}$ V cm^{-1}. The above-barrier ionization in such a field is rather strong and leads, in turn, to a further rise in the field strength. Thus, fields created at the beginning of ionization 'ignite' the cluster and promote its further ionization (hence, the name of the mechanism).

One more mechanism of electron emission from the cluster surface is attributed to usual thermoelectronic emission. It is described [3] by the Richardson–Dushman formula for the thermionic current from the spherical surface of the cluster (in atomic units) [92, 93]:

$$\frac{\mathrm{d}Z'}{\mathrm{d}t} = A_0 T_\mathrm{e}^2 4\pi R^2 \exp\left(-\frac{I_{Z'}}{T_\mathrm{e}}\right) . \tag{3.19}$$

Here, $A_0 = 1/(2\pi)^2$ is the so-called Richardson parameter, and the quantity $I_{Z'} = Z'/R$ is the ionization potential of a cluster ion with charge $Z' \gg 1$, when the work function may be neglected. The results [3] indicate that thermionic emission is a much more efficient mechanism of cluster ionization than field (cold) emission. In the above example of a sodium cluster with 10^6 atoms (and a total of 1.1×10^7 electrons) at the laser field intensity $I = 10^{15}$ W cm^{-2}, as many as 270,000 electrons are emitted. Nevertheless, the degree of cluster ionization remains low (about 2.4%).

Stochastic external ionization and strong stochastic heating of clusters are considered in Ref. [94]. The author believes that an electron randomly moving in an energy space can gain sufficient energy to overcome cluster potential and find itself in the continuum. In this case, external ionization of the cluster occurs. Estimates of the heating rate and external stochastic ionization time have been obtained. Stochastic heating is also feasible in the event of electron motion in a field of laser waves incident on and reflected from a cluster. Especially strong cluster heating by this mechanism is observed at relativistic intensities of laser radiation [94]. To close this section, it should be emphasized that yet other mechanisms of cluster heating and external ionization exist (see, for instance, Refs [3, 4, 8, 9]).

4. VUV free electron laser

High-power sources of X-ray radiation with the pulse length in the femtosecond range are now demanded by many scientific disciplines (physics, chemistry, biology, medicine, materials science, geophysics) [45, 95–97]. These sources allow chemical reactions between atoms to be observed in real time or instantaneous photographs of a complex molecule to be obtained. Such radiation characterized by extremely high intensity and tunable over a wide wavelength range is generated by high-gain free electron lasers [98–103]. Recent progress in accelerator technologies gives a reason to think that FELs are the most promising sources of VUV and X-ray radiation tunable across a broad spectral range [104–108]. FELs have recently been shown to produce radiation with a wavelength of 32 nm and a pulse length of 25 fs [50–52], as well as with 13.3 nm and a pulse length of around 10 fs [53]. It is expected to induce emission at a wavelength of 6 nm [109] in the near future, and at 0.1–0.15 nm by 2010–2012 [104] (see Section 5.5.3). Laser radiation is characterized by a rather high degree of coherence, and peak power of laser pulses amounts approximately to 1 GW [50, 110, 111]. The first successful experiments with such lasers yielded information on their radiation characteristics [50, 110, 111] and applications for excitation of atomic and cluster beams [51–53, 112]. Their use in other physical experiments was reported in Refs [53, 113, 114]. Results of the studies [113, 114] (see also Ref. [115]) indicate that intense pulses of VUV radiation from FELs may be utilized in many research and applied fields.

4.1 Principles of operation of a free electron laser

Let us consider the principles of operation of a high-gain FEL producing pulses in the UV spectral region, exemplified by the one based on the electron synchrotron built near Hamburg, Germany in the framework of the TESLA (TeV-Energy Superconducting Linear Accelerator) international project [49, 50, 110, 111, 116]. This project is being implemented jointly by 39 institutions in 9 countries, including Germany, France, Italy, the USA, and Russia [49, 50]. The aim of the project is to build up a 500 GeV (in the center-of-mass system) e^+e^- linear collider combined with an X-ray laser [96]. The main components of this FEL are an accelerator generating a high-energy bright electron beam and an undulator magnet. Electrons propagate in the undulator at relativistic velocities along an oscillatory path under the action of a periodic sequence of transverse magnetic fields. They emit radiation into a narrow band in the vicinity of the resonant wavelength $\lambda_{\rm ph}$ given by the relationship

$$\lambda_{\rm ph} = \frac{\lambda_{\rm u}}{2\gamma^2}\left(1 + \frac{K^2}{2}\right), \tag{4.1}$$

where

$$\gamma = \frac{E_{\rm e}}{m_{\rm e}c^2} \text{ is the electron relativistic factor, and}$$

$$K = \frac{eB_{\rm u}\lambda_{\rm u}}{2\pi m_{\rm e}c} \text{ is the undulator parameter.}$$

Here, $E_{\rm e}$ is the electron energy, $m_{\rm e}$ is the electron rest mass, e is the elementary charge, c is the speed of light in vacuum, $\lambda_{\rm u}$ is the undulator period, and $B_{\rm u}$ is the peak magnetic field in the undulator.

Interactions between the electrons and radiation generated in the undulator account for large gains of the FEL ($\geqslant 10^3 - 10^4$). Due to this, an FEL can be employed to obtain much more intense radiation compared with synchrotron emission. If the charge density of the electron beam is sufficiently high and the undulator is long enough, this interaction induces a periodic charge density oscillation in the electron bunch (beam) with the period given by the resonance wavelength $\lambda_{\rm ph}$. Once this 'microbunching' has been induced, many of the electrons start to radiate coherently at the resonant wavelength, thus increasing the radiation intensity and, in turn, the electron density modulation depth.

This mechanism leads to an exponential growth in radiation intensity along the undulator. The high-gain FEL considered here achieves laser effect and gain saturation within a single pass of the electron beam through the undulator [98–103]. Therefore, this laser does not require a set of mirrors as is the case in conventional lasers or in a low-gain FEL. In other words, the high-gain FEL is a very convenient source of radiation in the far UV region where suitable mirrors are not available. The lasing process in a FEL can be initiated by spontaneous undulator radiation, and the FEL works then in the so-called SASE (Self-Amplified Spontaneous Emission) mode [49, 102, 103, 116] without needing an external trigger signal.

Radiation power in the SASE mode grows exponentially with distance z along the undulator:

$$P(z) = AP_{\rm in}\exp\left(\frac{2z}{L_{\rm g}}\right), \tag{4.2}$$

where $L_{\rm g}$ is the radiation field amplification length, $P_{\rm in}$ is the power, and A is the coupling factor [101, 102]. In the case of an ideal electron beam in the one-dimensional theory of FELs, one finds $A = 1/9$ [49]. Because there are no tunable lasers in the short-wave region, the initial driving signal $P_{\rm in}$ is the spontaneous undulator radiation emitted in the inlet section of the device.

The SASE FEL considered in this section is capable of providing a peak brilliance (the photon flux per given frequency band and unit volume of the phase space) at least eight orders of magnitude higher than that with synchrotron radiation generated in storage rings [50, 97]. The half-height pulse length of such radiation is around 100 fs, and almost complete transverse coherence of the radiation is realized. Two major advantages of an FEL are revealed by relationship (4.1): the tunability of the wavelength by varying the electron energy or the magnetic field intensity, and the possibility of achieving a very short photon wavelength at high electron energies. The shortest wavelength achieved in this mode of operation up to now has been 13.3 nm [53], which was successfully used in experiments [53].

4.2 Main FEL elements and characteristics

Since the first observation of FEL generation in the SASE mode [49], the laser's elements and characteristics have been constantly improved [49, 50, 110, 111]. First and foremost, this is necessary for the achievement of maximum gain and generation in a shorter wave range [50, 104, 109]. Maximum gain and its saturation have already been achieved [49, 116], while generation was observed at a wavelength of 13.3 nm [53]. The elements and assembly of an FEL are schematically shown in Fig. 3. Electron beams are produced in the photoinjector (electron gun) by a train of laser pulses [117]

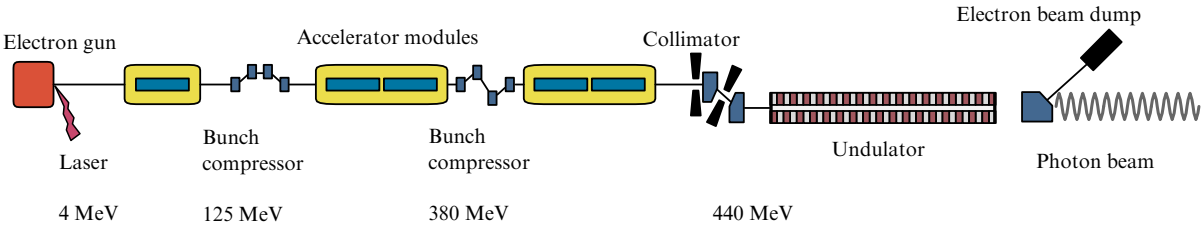

Figure 3. Schematic of the VUV free electron laser at the Hamburg linear accelerator [50].

Table 3. Main characteristics of the VUV free electron laser [49, 50, 110, 111].

Electron beam	
Beam energy, MeV	240 – 440
Beam (bunch) charge, nC	2.7 – 3.3
Charge of the beam emitting section, nC	0.1 – 0.2
Peak current, kA	1.3 ± 0.3
Root-mean-square deviation of the energy, keV	150 ± 50
Undulator	
Period λ_u, cm	2.73
Peak field, T	0.47
Mean β-function, m	1.2
Magnet length, m	13.5
Laser radiation	
Wavelength, nm	13.6 – 180
Pulse energy, μJ	30 – 100
Half-height pulse length, fs	50^{+50}_{-20}
Peak radiation power, GW	1
Mean radiation power, mW	up to 5
Half-height spectrum width	1 % of the wavelength
Spot size at the undulator output, μm	250
Half-height radiation divergence, μrad	130 ± 30

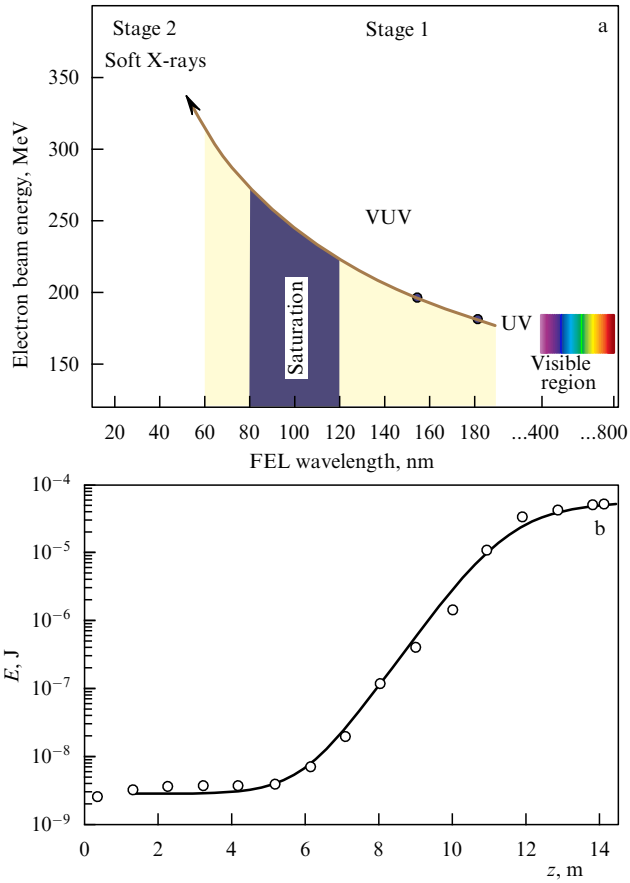

Figure 4. (a) Region of VUV-FEL wavelength tuning by varying the electron beam energy. After the beam energy reaches 1 GeV (stage 2), the laser starts to generate in the soft X-ray range [111]. (b) Mean energy in a FEL pulse depending on the undulator's active length. Circles — experimental results, solid line — results of numerical calculations using the parameters presented in Table 3 [111].

and accelerated to the energy of 445 MeV at the linear accelerator [118]. Beam charges between 0.5 and 1 nC were used. At intermediate energies of 125 and 380 MeV, the electron bunches are longitudinally compressed [119], thereby increasing the peak current from the initial 50 – 80 A to approximately 1 – 2 kA as required for FEL operation. The 30-m long undulator [120] consists of NbFeB permanent magnets with the fixed gaps of 12 mm, a period length $\lambda_u = 27.3$ mm, and a peak magnetic field $B_u = 0.47$ T. The two-pole magnet at the undulator output deflects the electron beam into a damp, while the FEL radiation propagates to the measurement room. The main characteristics of the laser are presented in Table 3.

The FEL operation demands a bunched electron beam of extremely high quality, specifically high peak current, a small emittance, a small velocity spread, and a short bunch length. Such a beam can be produced at linear but not circular accelerators. The electron injector consists of a laser-driven photocathode in a radio-frequency cavity operating at 1.3 GHz with a peak accelerating field of 40 MV m^{-1} at the cathode [117]. The Cs_2Te cathode is illuminated by a Gaussian-shaped UV laser pulse of 4 ps duration generated in a mode-locked solid-state laser generating a train of pulses. The laser pulse is synchronized with a radiofrequency pulse.

The electron injector section is followed by a total of five 12.2-m long accelerating modules (Fig. 3) which provide the beam energy of roughly 440 MeV required for the FEL operation at a 32-nm radiation wavelength according to Eqn (4.1). The accelerator is actually capable of providing even higher energies for electrons; it makes possible laser radiation emission in a range of about 10 nm [53]. The undulator system is divided into 6 segments, each 4.5 m long. Intervals of 60 cm between the segments contain quadrupole magnets for electron beam focusing and diagnostics. A very close overlap between the electron beam and the radiation field generated inside the undulator is indispensable for normal FEL operation, hence the necessity of thorough adjustment of all the system's elements. The results of experiments [50] indicate that the fields formed in all undulator modules are of very high quality; due to this, the expected deflections of electron orbits from ideal ones do not exceed 10 μm [50].

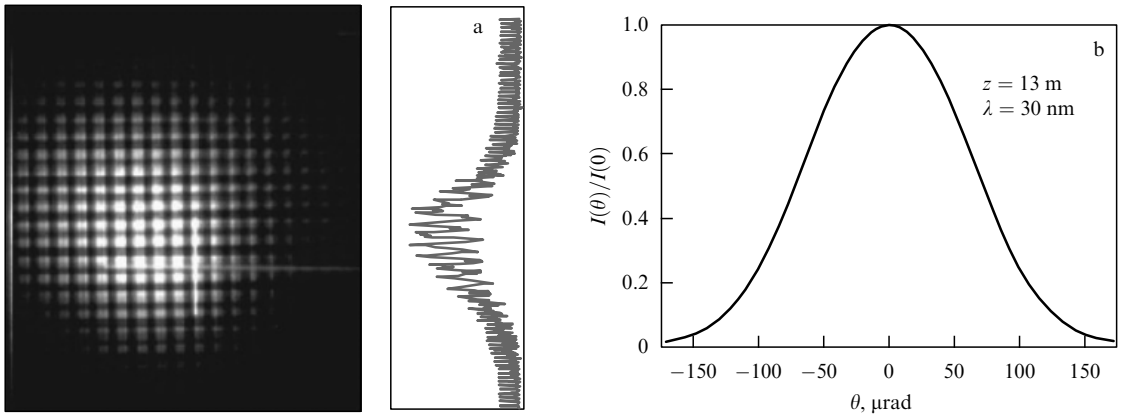

Figure 5. (a) Image of a single radiation pulse from a VUV FEL on a Ce:YaG crystal behind the gold wire mesh of a multichannel detector. (b) Simulated [119] angular divergence of the FEL radiation intensity in the far zone [50].

4.3 FEL radiation properties

The main characteristics of FEL radiation (gain coefficient, angular divergence, pulse energy and length, pulse energy dispersion, and pulse spectral width) were investigated both in experiment [49, 50, 111] and by simulation [121–123]. An FEL was operated for the first time in the SASE mode in 2000 [49, 116]. The gain coefficient during a single pass was found to exceed 10^3 and even 10^4. A variation in the accelerator energy revealed wavelength tuning within a rather broad range from 80 to 180 nm (Fig. 4a). Thereafter, a maximum laser gain was achieved and the gain coefficient was shown to saturate across the entire range [110, 111]. Figure 4b demonstrates the dependence of the measured energy in the radiation pulse on the active length of the undulator, defined as the distance over which electron and photon beams overlap. These measurements were made at a wavelength of 98 nm [111]. Figure 4b clearly demonstrates the exponential growth of the FEL energy (power) with the undulator length in the SASE regime. For the characteristic length of power amplification, the above dependence gives $L_g = 67 \pm 5$ cm. The pulse energy ranges from 10 to 100 μJ depending on the radiation wavelength and the electron beam charge. The estimated pulse energy may be as high as 100μJ at a wavelength of 30 nm and an electron beam charge of 1 nC according to calculations [119, 122].

An important parameter of a laser beam is angular divergence (spatial coherence). Figure 5a shows an image induced by a laser pulse on a Ce:YAG crystal placed on the laser beam path behind the gold mesh of a multichannel detector. The mesh was mounted 18.5 m downstream from the undulator exit aperture. The wires are clearly visible. From the wire spacing of 0.31 mm, image analysis yields a half-height laser spot size of 3 mm. This corresponds to a beam half-height angular divergence of 130±30 μrad, the error being mainly due to the uncertainty of the longitudinal position of the point at which the laser process starts from spontaneous noise. There is a good agreement with the simulated angular divergence (Fig. 5b). The observed angular divergence is comparable to the diffraction divergence, which is a clear indication of a high degree of transverse coherence of the laser beam [50].

Radiation pulses of the SASE FEL are characterized by marked energy dispersion. Figure 6 depicts the measured energies of many successive pulses. A large fluctuation is seen, which is to be expected since the amplification starts from shot noise. Theoretically, the laser pulse energy should fluctuate [49] in accordance with the gamma-distribution:

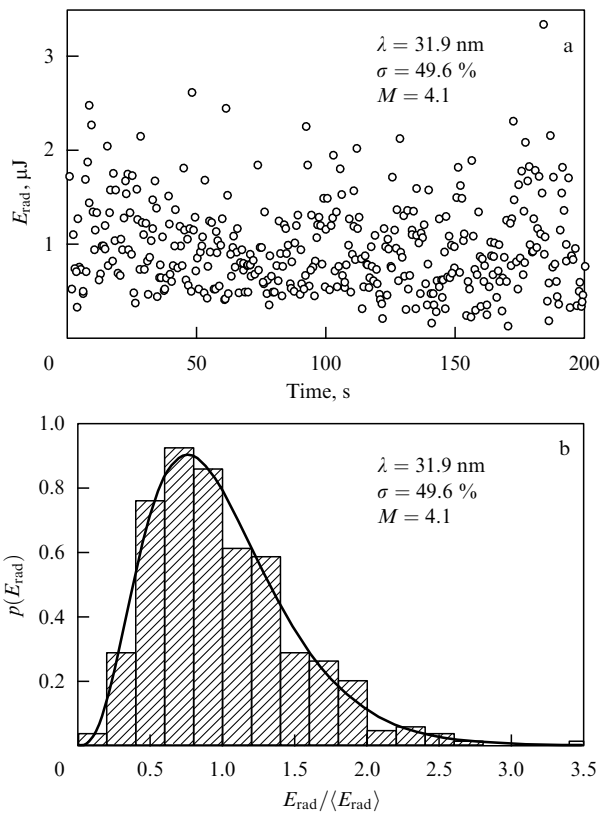

Figure 6. Measured FEL pulse energies for many successive pulses. (a) Pulse-to-pulse variation in FEL energy. (b) Measured probability distribution of the radiation energy (histogram). Solid curve represents the gamma-distribution [relation (4.3)] for $M = 4.1$, which is calculated from the variance of the pulse energy fluctuations illustrated in figure (a) [50].

$$p(E) = \frac{M^M}{\Gamma(M)} \left(\frac{E}{\langle E\rangle}\right)^{M-1} \frac{1}{\langle E\rangle} \exp\left(-M\frac{E}{\langle E\rangle}\right), \quad (4.3)$$

where

$$M = \frac{\langle E\rangle^2}{\langle (E - \langle E\rangle)^2\rangle},$$

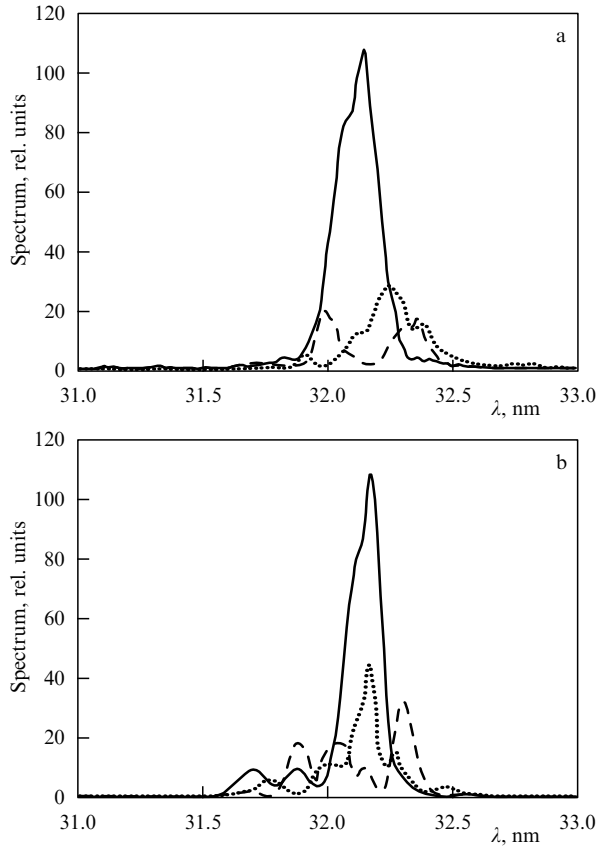

Figure 7. (a) Spectra of three single VUV-FEL radiation pulses. (b) Simulation of the spectral structure of the VUV FEL operating in the exponential amplification regime [119]. Shown are the results for three different pulses (solid, dashed, and dotted lines). Note that the number of spikes in the spectrum is on average equal to the number of spikes (coherent wave packets) in the time structure of the radiation pulse [50].

provided the FEL gain process is in the regime of exponential growth [103, 122]. Here, $\langle E \rangle$ is the mean photon energy, and Γ is the gamma-function. Parameter M is the inverse of the normalized variance of E. It defines the number of optical modes in the radiation pulse and provides a relationship between the number of spikes in the single-pulse generation spectrum and the fluctuations of pulse energy. The measured histogram in Fig. 6b fits nicely with the gamma-distribution (4.3) at $M = 4.1$.

The pulse length of laser radiation was found from measurements of the pulse spectral width (Fig. 7). The spectra of three pulses shown in Fig. 7a were taken with a grating spectrometer (0.04-nm resolution) equipped with an intensified CCD camera. The half-height pulse duration was obtained from the spectral width $\Delta\omega$ of the spikes in the single-pulse spectrum using the relation $\tau_{\rm rad} \cong 2\pi/(\Delta\omega) \cong 25 \pm 5$ fs. With the mean radiation pulse energy of 10 μJ, this corresponds to an average power of 0.4 GW for the FEL pulse and approximately 1 GW inside the spikes. Note that the FEL pulse duration can also be roughly estimated from the peak portion length of the electron bunch that equaled 50 fs in the experiments being described [50]. One more important parameter in many experiments is the brightness of laser radiation. For a VUV FEL emitting at a wavelength of 30 nm, the maximum brightness is close to 10^{28} photons/(s mm^2 mrad^2) in 0.1% of the bandwidth [50].

5. Cluster spectroscopy by intense pulses of VUV radiation

5.1 Early experiments. Absorption of radiation by clusters

5.1.1 Results of observations. The first experiments on cluster excitation by VUV emission from FELs were reported by Wabnitz et al. [124]. The authors investigated interactions of intense FEL radiation ($\lambda = 98$ nm) with xenon atoms and clusters. These objects were chosen because they can be ionized by single photons of a given wavelength with an energy of 12.7 eV, the ionization energy of xenon atoms being 12.13 eV [125]. The atoms and clusters were exposed to pulses of about 100 fs duration and an intensity from 4×10^{10} to 7×10^{13} W cm^{-2}. The resulting ions were detected by a time-of-flight mass spectrometer.

The ions exhibited very broad mass peaks (Fig. 8), suggesting their rather high kinetic energy associated with a Coulomb explosion of clusters. The number of ions with different charges and their kinetic energy strongly depend on the intensity of exciting radiation as displayed in Fig. 8 which presents mass spectra of the ions produced upon excitation of xenon clusters comprising 1500 atoms. At the highest intensity reached in this experiment, 7×10^{13} W cm^{-2}, ions with a charge of up to $Z - N_{\rm e} = 8$ ($N_{\rm e}$ is the number of

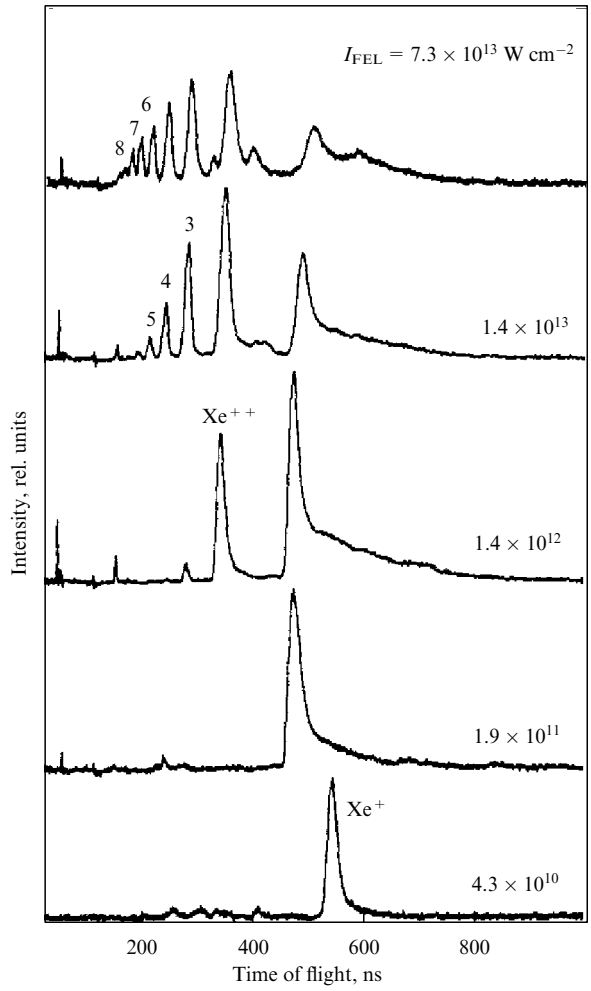

Figure 8. Time-of-flight mass spectra of Xe_N clusters ($N = 1500$), obtained after exposure to VUV pulses from an FEL at a wavelength of 98 nm and different intensities [124].

remained ion electrons) were obtained. The ion peak intensity corresponding to multiply charged ions dropped sharply with a decrease in exciting radiation intensity. For example, only singly charged Xe^+ ions with rather high kinetic energy were detected at the intensity of 2×10^{11} W cm^{-2}.

The strong intensity dependence of the signals clearly indicates that nonlinear optical processes predominate at the power levels being used. When the intensity grows from 2×10^{11} to 7×10^{13} W cm^{-2}, the average charge increases from 1 to about 2.5. This means that at the highest intensity each atom in a cluster of 1500 xenon atoms loses, on average, 2–3 electrons [124].

The mean kinetic energy of ions found from the time-of-flight measurements (Fig. 8) shows a strong dependence on the cluster charge and size. The kinetic energy of a Xe^{7+} ion is above 2 keV. In small clusters, it grows quadratically as their charge increases. Such a behavior provides strong evidence that the cluster disintegrates in a Coulomb explosion [126]. As follows from Fig. 8, up to a few hundred electron-volts of energy per atom are absorbed from the laser pulse field.

The effects in clusters excited by short-wave VUV radiation as described in Ref. [124] are surprising because a Coulomb explosion starts at an intensity as low as 10^{11} W cm^{-2}, or much smaller than is necessary for a Coulomb explosion in the IR region. Moreover, the frequency of exciting radiation is so high that the direct effect of the laser field on electron motion is insignificant [127]. The experiments being considered demonstrated that field ionization, a predominant process of cluster ionization by IR radiation, makes no contribution to the ionization process in the case of an FEL at 98 nm. Nor is the electron motion induced by the electric field of a laser pulse a critical factor in these experiments, and there must be no laser-induced direct ejection of electrons from the cluster. Consequently, additional processes and other ionization mechanisms need to be considered to gain greater insight into the absorption, ionization, and cluster explosion dynamics under excitation by UV radiation from an FEL.

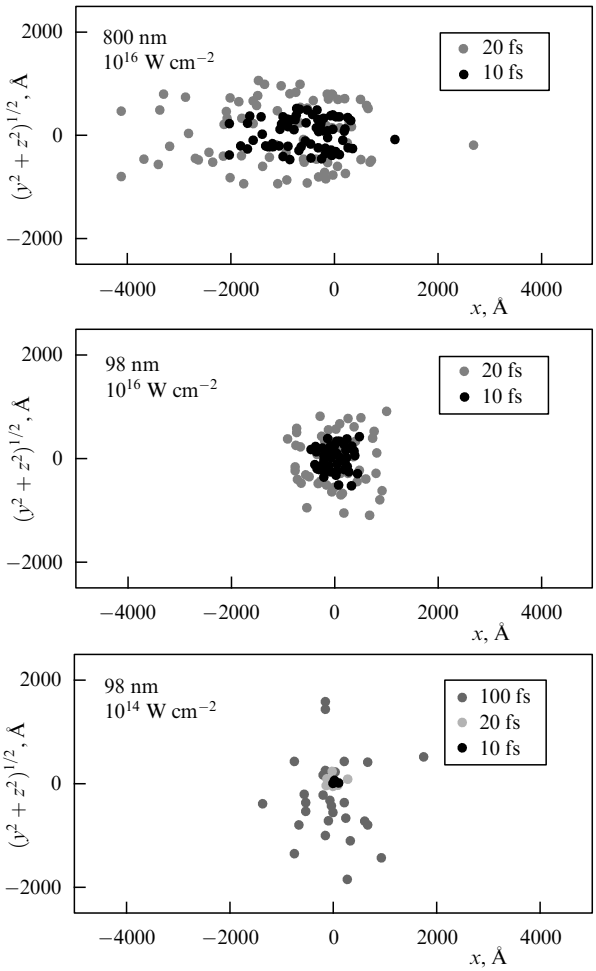

Figure 9. Results of calculations of electron motion and the ionization process for Xe_{13} clusters after their exposure to IR or soft X-ray radiation. Electron trajectories are computed for 100-fs laser pulses having a similar energy in both exposition regimes. Electrons are shown in the positions they occupied 10, 20, and 100 fs after the onset of exposure to the laser pulse. Laser radiation is polarized parallel to the x-axis [130].

5.1.2 Interpretation of results. The authors of Ref. [124] regarded cluster ionization as a two-step process in analogy with ionization by IR radiation [69, 128]. At the first stage, atoms in a cluster lose at least one electron each, which then start to move almost freely inside the cluster (internal ionization). At the second stage, electrons move off from the cluster to infinity (external ionization). Internal ionization is easy to account for by the fact that the FEL photon energy is higher than the Xe ionization energy. Therefore, valence electrons in a cluster may be supposed to change to excited states (conduction zone). At an intensity above 10^{13} W cm^{-2}, such a transfer takes the first several femtoseconds of the FEL pulse by virtue of a very large absorption cross section (30–50 Mb) [129].

In order to better understand radiation absorption processes and ionization mechanisms, the authors of Ref. [124] simulated motion of free electrons in Xe_{13} and Xe_{55} clusters, taking into account forces by which they are acted on by cluster ions and electrons and by the laser pulse field. It was found that electrons are isotropically emitted from the cluster at a laser wavelength of 98 nm and intensities of 10^{14} and 10^{16} W cm^{-2}, as opposed to typical experiments with optically-pumped lasers (800 nm, 10^{16} W cm^{-2}) where most electrons were emitted parallel to the polarization direction of the pulse electric field. This confirms the field ionization of clusters in the latter case. A similar result was obtained in Ref. [130] (Fig. 9). Conversely, the isotropic emission of electrons from a cluster in the case of their excitation by an FEL at 98 nm suggests the absence of field ionization. The authors argue that an electron is multiply scattered inside the cluster before leaving it; as a result, the cluster is strongly heated.

Also, the authors of Ref. [124] hypothesize that multiply charged ions form at the cluster surface by means of field ionization in the strong Coulomb field of intracluster ions [70, 91]. The electric field strength at the surface of a large high-charge cluster is usually 10–50 V Å^{-1} or almost 20 times the FEL field strength at an intensity of 10^{14} W cm^{-2}. For Xe^{8+} ions to form, the field strength should be around 30 V Å^{-1} [131]. The above line of reasoning explains the formation of multiply charged ions for cluster excitation by UV light from an FEL [130, 132–134]. However, it does not explain why such high-charge states are unobservable when xenon clusters are excited by intense IR pulses. It may be conjectured that the high-charge states of xenon clusters excited by FEL UV radiation are formed due to collisional ionization and thermalization of the clusters (see Section 5.4). Later studies [133] demonstrated that electrons emitted from a cluster are

characterized by the Boltzmann energy distribution and their mean temperature under UV excitation is only 30 – 40 eV, compared with 1 – 10 keV when excited by IR radiation at 800 nm. Thus, the data obtained suggest different mechanisms of cluster ionization by IR and UV radiation; they also demonstrate the high efficiency of cluster excitation by FEL UV radiation.

5.2 Photoelectron spectroscopy of clusters

Photoelectron spectroscopy, as opposed to mass spectroscopy, gives additional and more detailed information about nonlinear processes developing when atoms and clusters are excited by intense radiation. Suffice it to say that the observation of high-energy electrons (up to 3 keV) during cluster excitation by optical pulses is in line with the description of cluster–radiation interaction in the framework of the so-called cluster nanoplasma model [1, 3, 135]. An essential question arises which concepts for the description of the absorption and ionization of matter excited by pulses of visible wavelengths are applicable to the case of its excitation by intense VUV pulses. The answer is of importance not only for cluster physics but also for understanding interactions between matter and radiation. Investigations into the photoemission of electrons and ions may clarify this problem by providing information on ionization mechanisms in the short-wave limit.

A detailed study [133] of cluster ionization by intense VUV radiation from an FEL operating at 95 nm used photoelectron spectroscopy and the computations in the Thomas – Fermi model [126]. Laser radiation intensity was $\sim 4 \times 10^{12}$ W cm^{-2}, while Ar_N and Xe_N clusters contained 70 – 900 atoms each. The clusters formed during supersonic gas outflow from a nozzle. Their mean size was changed between 70 and 900 atoms by varying gas pressure above the nozzle [136]. FEL radiation ($\hbar\omega \cong 13$ eV, pulse length ~ 100 fs, and pulse energy 0.3 – 5 μJ) was focused by an elliptical mirror onto a cluster beam; the spot size was roughly 20 μm. Maximum radiation intensity at the focus point reached 10^{14} W cm^{-2}. Electrons arising from cluster–radiation interaction were detected in the laser polarization direction by the microchannel plate of the time-of-flight mass spectrometer. This method permitted analyzing electron kinetic energy in a range from a few electron-volts to several kiloelectron-volts. The experimental electron distribution curve $I(t)$ was converted to the energy distribution curve $I(E)$, taking into account that $I(E) \propto t^3 I(t)$. Figure 10 displays photoelectron spectra taken from Ar_{300} clusters (a), Ar atoms (b), Xe_{70} clusters (c), and Xe atoms (d) irradiated by VUV pulses at an intensity of $\sim 4 \times 10^{12}$ W cm^{-2}. At such an intensity, clusters of rare gases totally disintegrate into multiply charged atomic fragments in a Coulomb explosion [124, 132].

Interactions of clusters with VUV radiation give rise to a broad distribution of photoelectrons over kinetic energy. The electron energy decreases roughly exponentially in accordance with the relationship

$$w(E_e) = w_0 \exp\left(-\frac{E_e}{E_0}\right), \tag{5.1}$$

where $E_0 \sim 8.5$ eV (for Ar), and ~ 8.9 eV (for Xe). The Ar_N spectrum exhibits a quite apparent asymmetric peak at 10.4 eV, besides these 'thermal' electrons. It can be concluded from the comparison of photoelectron spectra of Ar_N clusters and Ar atoms (Fig. 10b) that this peak is associated with two-photon ionization of neutral Ar atoms present in the cluster

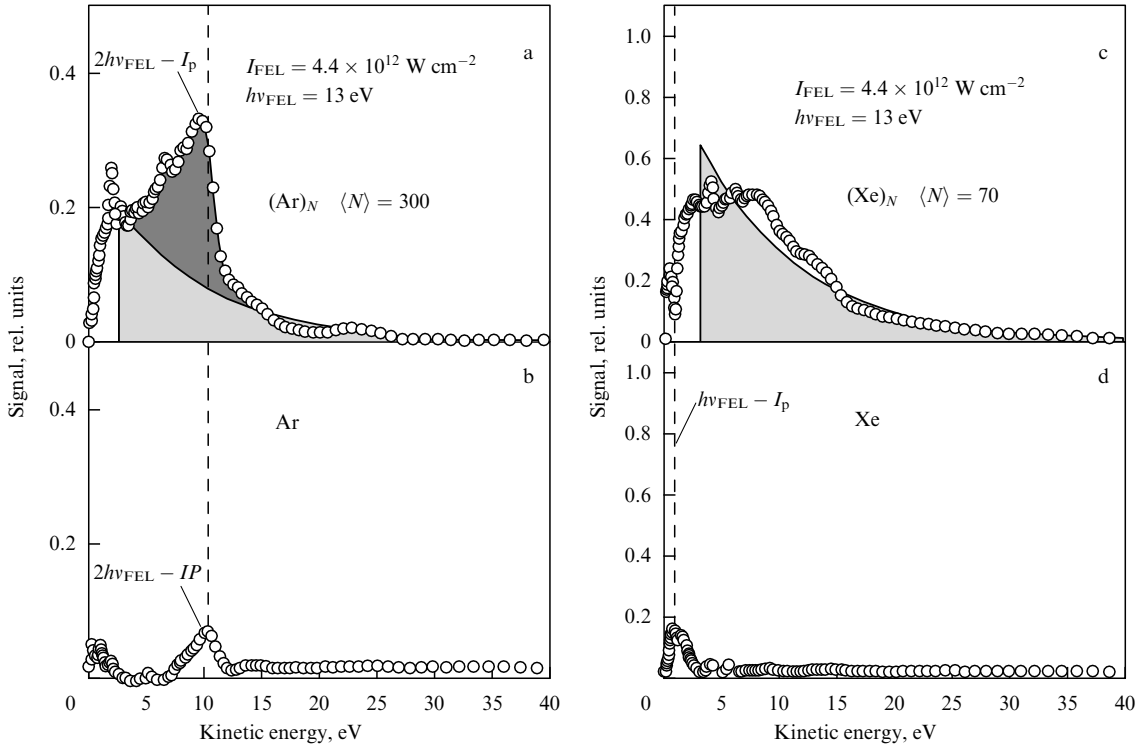

Figure 10. Photoelectron spectra of Ar_{300} clusters (a), Ar atoms (b), Xe_{70} clusters (c), and Xe atoms (d) irradiated by FEL radiation pulses ($\lambda = 95$ nm, $\tau_p = 100$ fs) at an intensity of 4.4×10^{12} W cm^{-2} [133]; I_p — ionization potential of Ar (a, b) and Xe (c, d) atoms.

beam. Note that the energy of an FEL photon is significantly lower than the first ionization potential of Ar atoms (15.76 eV) but higher than that of Xe atoms (12.13 eV). This means that two photons are needed to ionize an Ar atom, and only one to ionize an Xe atom. Studies on the relationship between cluster size (Ar_{300} and Ar_{900}) and kinetic energy distribution of emitted electrons at an identical intensity of FEL pulses showed that the electron energy increases with cluster size [133].

The main result obtained in Ref. [133] resides in the discovery of a small maximum kinetic energy ($\leqslant 40$ eV) of electrons emitted from clusters exposed to VUV radiation pulses from an FEL. The energy distribution roughly corresponds to the thermal (Boltzmann) distribution, in contrast to the case of cluster excitation by high-intensity optical pulses when clusters emit electrons with an energy of several kiloelectron-volts [1, 3, 9, 135].

In order to obtain a deeper insight into the ionization process, in particular, the formation of the thermal distribution of emitted photoelectrons, the authors of Ref. [133] made calculations for Ar_{55} clusters based on a nonstationary Thomas–Fermi model [126]. In this model, oscillations of an electron cloud inside a cluster are regarded as the motion of a fluid having a certain density and velocity. We shall consider the main results of this work without going into calculation details. Figure 11a, b presents calculated spectra of the kinetic energy of free electrons emitted in an explosion (expansion) of clusters irradiated by VUV pulses at peak intensities 10^{14} and 10^{12} W cm^{-2}. The exponential (thermal) character of electron energy distributions is clearly apparent; they correspond to electron gas temperature $E_0 = 6.6 \pm 0.4$ eV (a) and 4.2 ± 0.2 eV (b). The mean kinetic energy of photoelectrons shifts toward higher values with a rise in the exciting pulse intensity. The computed electron temperature at an intensity of 10^{12} W cm^{-2} is roughly two times lower than the observed one. The authors of Ref. [133] attribute this difference to the fact that calculations were made (to save computer time) for a smaller cluster Ar_{55} in comparison with Ar_{300} used in the experiment (the kinetic energy of electrons being much greater for bigger clusters) [133].

The photoelectron spectra presented in Fig. 11a, b give direct experimental evidence of heat-activated emission of electrons. Such a process has recently been predicted theoretically [130], even if disregarding ion dynamics. The ionization process can be interpreted as follows. The Keldysh parameter during cluster excitation by VUV radiation from an FEL is $\gamma \gg 1$; therefore, multiphoton ionization of cluster atoms takes place [124] as also confirmed by experimental examination of two-photon ionization of neutral Ar atoms (Fig. 10b). For this reason, internal ionization of clusters at the onset of their interaction with a VUV pulse occurs first and foremost via two-photon (for Ar clusters) or single-photon (for Xe clusters) absorption by intracluster atoms. A few femtoseconds later a plasma forms, and the overwhelming majority of the emerging electrons are bound by Coulomb forces to the dense ionic nucleus of the cluster. In this case, energy deposition is mainly controlled by collisional heating of the plasma [74, 137, 138], which is more efficient in large clusters and at higher intensities (Fig. 11a, b). Quasi-free electrons inside the cluster receive sufficiently high energy, enabling them to overcome the potential barrier and leave the dense cluster ionic nucleus. Thus, external cluster ionization occurs.

Additional data on ionization dynamics were obtained by calculating the number of emitted electrons depending on

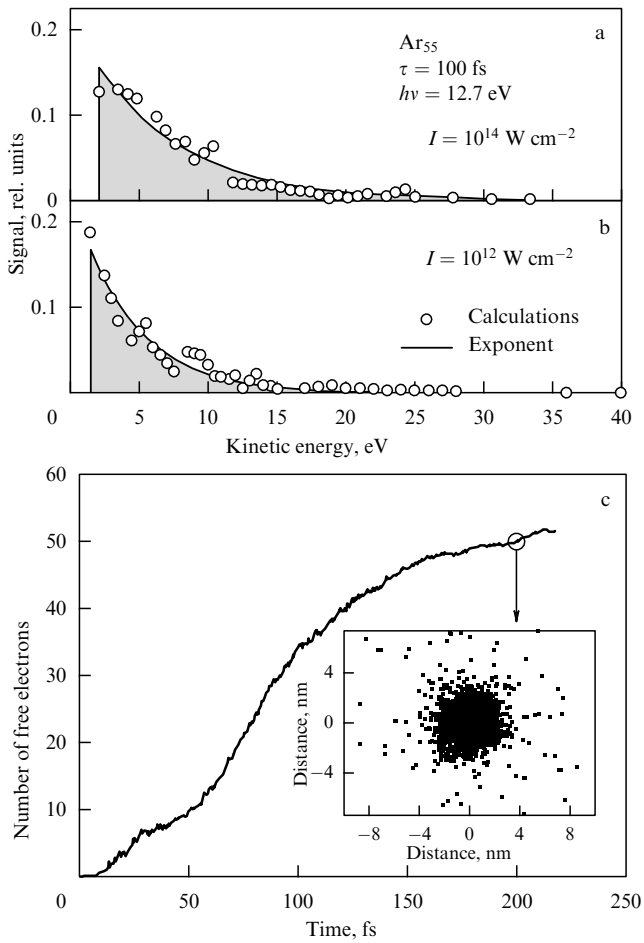

Figure 11. Theoretical photoelectron spectra of Ar_{55} clusters exposed to laser pulse radiation with peak intensities of 10^{14} W cm^{-2} (a) and 10^{12} W cm^{-2} (b) computed based on the nonstationary Thomas–Fermi model. Exponential dependences show adjustable values for electron kinetic energy distributions [133]. (c) Calculated number of emitted electrons depending on cluster exposure time at 10^{12} W cm^{-2}. The inset presents two-dimensional projection of pseudoparticles showing electron density distribution 'as of the time of the snapshot' at the end of the laser pulse [133].

exposure time (Fig. 11c). Calculations were made for the radiation intensity of 10^{12} W cm^{-2} (as shown in Fig. 11b). The dependence thus obtained clearly indicates that at the onset of a VUV pulse, when the plasma has already formed, the strong Coulomb attraction practically blocks the escape of electrons from the cluster. Such a behavior is altogether different from the case of cluster excitation in the visible range, when a major portion of electrons are instantaneously 'pushed out' from the cluster surface by the leading edge of the laser pulse in the laser polarization direction as a result of field ionization [130, 135] (see Section 5.1 and Fig. 9).

As seen in Fig. 11c, most electrons are emitted after a lag, i.e., after the FEL pulse has passed and ion expansions have started. In large clusters ($N > 1000$), a major part of the electrons are emitted after the switch-off of the pulse. The inset to Fig. 11c shows a two-dimensional projection of pseudoparticles simulating electrons. This snapshot obtained 200 fs after the onset of the pulse clearly shows that electron emission proceeds further in time and has an isotropic nature (see also Section 5.1 and Fig 9). These findings are interpreted as follows. The results of calculations suggest that electrons undergo multiple scattering inside

a cluster before external ionization causes statistical redistribution of the energy between electronic degrees of freedom [139]. The FEL pulse duration being small compared with the characteristic electron–phonon coupling time (ca. 10^{-12} s), the electron temperature established immediately after pulse excitation is considerably higher than the ion temperature because the absorbed laser energy is most of all spent to ionize atoms and heat electron gas. Electrons located near the cluster surface and belonging to the high-energy tail of the temperature distribution may break away from the cluster in the course of Coulomb expansion due to the lowering of the Coulomb barrier. This accounts for the delayed release of thermally excited electrons, which can be referred to as thermal electron emission, in contrast to thermionic emission characterized by equilibrium between electronic and nuclear degrees of freedom [140].

Photofragmentation of Ar_N clusters ($N \sim 10^3$) during irradiation by 25-fs FEL pulses at a wavelength of 32 nm ($\hbar\omega = 38$ eV) and an intensity of 3×10^{13} W cm^{-2} has recently been investigated by time-of-flight spectroscopy [141]. The energy of emitted photoelectrons was found to vary from 2 to 23 eV, and photoelectron dynamics differed from that of excitation at a wavelength of 95 nm ($\hbar\omega = 12.7$ eV). The authors observed intense instantaneous emission of electrons from the clusters, in addition to the slow thermal electron emission characteristic of cluster excitation at $\lambda = 95$ nm. This fast emission involved electrons that had acquired rather high kinetic energy ($E_e = \hbar\omega - I_p \approx 22.2$ eV) through primary atomic ionization and surmounted the potential barrier of the cluster ion.

To conclude this section, the available data indicate that the excitation of atomic clusters by intense VUV pulses of FEL radiation results in a rather low kinetic energy of electrons emitted from the clusters. At a peak laser intensity of $\sim 4 \times 10^{12}$ W cm^{-2}, kinetic energy distribution of emitted electrons decreases exponentially to 30–40 eV. The characteristic electron temperature is below 10 eV. Calculations based on the nonstationary Thomas–Fermi model taking into account the effects of collisional heating of electrons confirm the cluster ionization to be a thermal electron emission. Low-energy electrons leave a cluster after a time lag. The emission of electrons is isotropic and independent of laser polarization. These evidences are in obvious conflict with the results of experiments on cluster excitation at optical frequencies, when the following two processes take place: (1) field ionization with the release of surface electrons at the leading edge of a laser pulse, and (2) delayed emission of high-energy ($\geqslant 1$ keV) electrons described by a nanoplasma model. Also, different ionization mechanisms explain why electrons emitted during interaction between clusters and VUV radiation have a much lower energy than electrons released from clusters excited in the visible range.

5.3 Photoion spectroscopy of clusters

The excitation of Ar_N clusters ($N = 170-900$) by intense VUV-FEL pulses was investigated in Ref. [132] by photoion spectroscopy. The radiation wavelength of the laser could be tunable in a rather broad range from 80 to 120 nm, which allowed emission to be tuned to resonance with the absorption bands of bulk and surface excitons in argon clusters, falling at 100 nm and 105 nm, respectively [142]. This approach made it possible to study the effects of the excitation energy on cluster absorption in the case of resonant and nonresonant excitation. Argon clusters were formed upon supersonic gas outflow from a conical nozzle with an outlet orifice of diameter 100 μm and a total spread angle of 30°. Mean cluster size ($N = 170-900$) was varied by changing gas pressure above the nozzle. FEL pulse energy ranged from 0.3 to 5 μJ, while the pulse duration varied around 50 fs. Laser light was focused onto a 20-μm spot. Under these conditions, maximum radiation intensity at the focus amounted to 10^{13} W cm^{-2}. The ions thus produced were detected in a time-of-flight mass spectrometer with a microchannel plate as the detector.

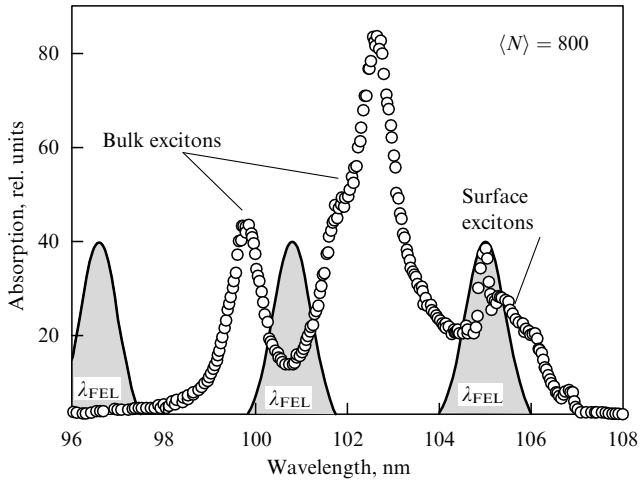

Figure 12. Photoabsorption spectrum of Ar_{800} clusters obtained in Ref. [142]. FEL radiation could be tuned to or out of resonance with surface and bulk excitons [132].

The dependence of the energy deposited into a cluster on a concrete electronic structure corresponding to bulk and surface atoms [142] was studied by tuning the laser wavelength to the respective absorption bands of the cluster, as shown in Fig. 12 for Ar_{800} clusters. The spectrum depicted in Fig. 12 was obtained in Ref. [142] by the excitation of fluorescence using synchrotron radiation. Fixing the FEL radiation wavelength at 105, 100.8, and 96.6 nm made it possible to implement site-selective excitation of intracluster atoms, notwithstanding a rather broad laser emission spectrum (ca. 0.5–1% of the radiation wavelength).

Figure 13a displays time-of-flight spectra obtained by exciting argon clusters at three different wavelengths and identical peak intensities around 1.5×10^{13} W cm^{-2}. It can be seen that the Ar_{900} clusters totally disintegrate into multiply charged atomic fragments. A good few photons are absorbed from the laser field. Notice that at least two FEL photons are needed to ionize an argon atom, since its ionization potential amounts to 15.76 eV [125]. The distribution of ionic fragments Ar^{q+} over kinetic energies can be deduced from the ions' time of flight. It directly provides information on the efficiency of energy deposition into the clusters. At a laser peak intensity of about 10^{13} W cm^{-2}, cluster ionization goes independent of the exciting radiation wavelength, meaning that the electronic structure of the initially excited states has no effect on the ionization process at such intensity. Energy depositions are identical in cases of resonant excitation of bulk or surface excitons and of nonresonant cluster excitation, as seen in Fig. 13a from the similar kinetic energy distributions of Ar^{q+} fragments. Conversely, mass spectra are significantly different at a low peak radiation intensity of about

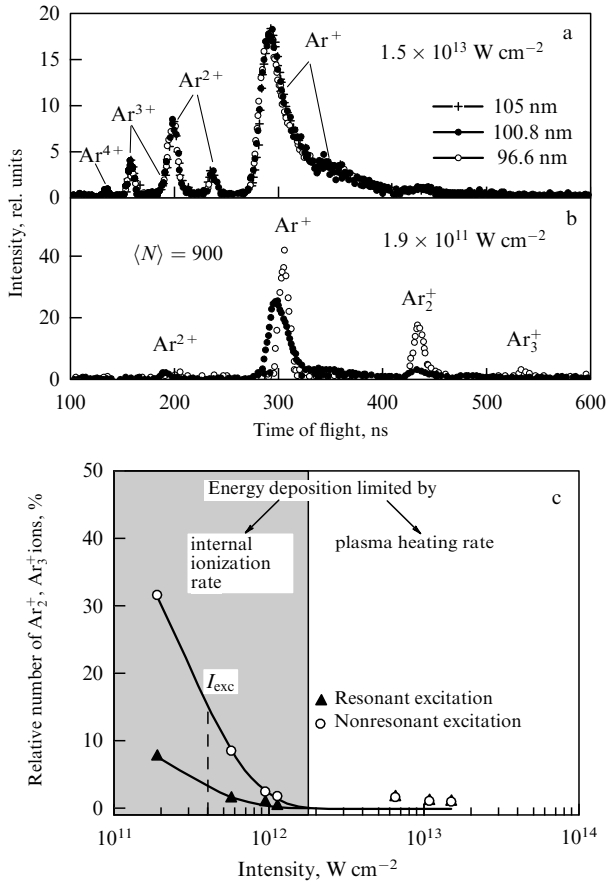

Figure 13. Time-of-flight mass spectra taken after exposure of Ar_{900} clusters to FEL emission at three wavelengths (excitation of surface and bulk excitons or nonresonant excitation) and different radiation intensities: 1.5×10^{13} W cm^{-2} (a), and 1.9×10^{11} W cm^{-2} (b). The spectra were derived from the region lying 3 mm from the lens focus [132]. (c) Relative number of Ar_2^{+} and Ar_3^{+} ions formed during irradiation of Ar_{900} clusters depending on laser radiation intensity. Resonant excitation of bulk excitons is compared with nonresonant excitation [132].

10^{11} W cm^{-2} achieved by displacing the cluster beam 3 mm from the focal point (Fig. 13b). Nonresonant excitation produces peaks of large cluster fragments (Ar_2^{+}, Ar_3^{+}).

These results can be understood bearing in mind that a Coulomb explosion of clusters is under the control of the ionization process and of the cluster plasma heating rate. Therefore, the total energy absorbed from a laser pulse is essentially dependent on the internal ionization rate; it determines both density and heating rate of the plasma being formed (see Sections 3.3 and 3.4). In this context, the energy absorbed by argon clusters at a laser peak intensity of about 1.5×10^{13} W cm^{-2} is controlled largely by the plasma heating rate, whereas the limiting factor of energy absorption at low peak intensity (1.9×10^{11} W cm^{-2}) is the internal ionization rate for the initial part of the laser pulse. In these conditions, the electronic structure of the clusters starts to play an important role, which accounts for the large difference between absorption cross sections in cases of resonant and nonresonant excitation. In the latter case, the absorbed energy is smaller; as a result, mass spectra exhibit peaks corresponding to large fragments. When the number of absorbed photons exceeds a certain critical value, ion peaks of Ar_2^{+}, Ar_3^{+} lower because the clusters undergo fragmentation, mostly into atomic ions.

Figure 13c depicts the dependences of the relative content of Ar_2^{+} and Ar_3^{+} ions in the mass spectrum of Ar_{900} clusters on peak intensity of exciting radiation in resonant and nonresonant excitations of cluster bulk excitons. When the intensity is higher than that of exciton absorption saturation, $I_{exc} \sim 4 \times 10^{11}$ W cm^{-2}, resonant excitation leads to the complete disintegration of the cluster. On the other hand, nonresonant excitation at the same intensity produces a mass spectrum showing a large number of Ar_2^{+} ions. The two curves coincide at a somewhat higher intensity, $\sim 1.8 \times 10^{12}$ W cm^{-2}. This means that strongly absorbing exciton states no longer accelerate internal ionization at high radiation intensities. Therefore, it may be supposed that during the first femtoseconds in this regime each atom in an argon cluster becomes singly ionized due to the simultaneous absorption of two photons from the laser pulse field. Thus, effects observed at high intensities can be explained in the following way. Initial ionization of cluster atoms gives rise to a plasma initially containing one free electron per ion. At this stage, the energy deposition critically depends on ion density and average charge per ion. Quasi-free electrons receive via collisional heating the energy sufficient to overcome the potential barrier and leave the dense cluster nucleus in the course of thermal electron emission [124].

In order to determine the mean charge state of a cluster and the total energy it absorbed, the authors of Ref. [132] simulated time-of-flight mass spectra obtained in experiments which were based on measurements of the mean kinetic energy and distribution width of ion fragments ($Ar^{+} - Ar^{6+}$). Figure 14a presents the results of calculations for Ar_N clusters of 170 atoms exposed to FEL irradiation in the absorption band of bulk excitons at an intensity of 3.2×10^{13} W cm^{-2} and a wavelength of 100.8 nm. Experimental findings are displayed in Fig. 14b for comparison. Calculated and observed values appear to be in fairly good agreement. Calculations indicate that each atom in the cluster loses two electrons and absorbs up to 20 photons during a 50-fs long FEL pulse. When it is assumed that clusters go through heating in the process of successive absorption of single photons, then this will correspond to the average absorption cross section $\sigma_{exp} = 24.1$ Mb per atom.

In order to elucidate mechanisms of energy absorption in clusters exposed to VUV radiation, the authors of Ref. [132] performed calculations of classical electron motion under the action of an intense laser pulse by the molecular dynamics method (MDM) [130] in accordance with the model proposed in Ref. [70]. The model includes the effects of collisional heating of quasi-free electrons and ions inside the cluster, such as inverse bremsstrahlung and plasma resonant absorption [143]. Calculations were made for an argon cluster of 147 atoms containing two quasi-free electrons per atom. The electrons travel in the cluster as point charges under the action of Coulomb forces and a laser field. The time dependence of the total energy absorbed by 294 electrons being propelled by the laser field at an intensity of 3.2×10^{13} W cm^{-2} and a wavelength of 100.8 nm is shown in Fig. 14c. By way of comparison, Fig. 14c also presents calculated data for a wavelength of 800 nm. In the case of the large (low frequency) wavelength, electrons are more easily entrained by the laser field and, as a result, more efficiently absorb energy due to collisional heating. During excitation at 100.8 nm, the laser field oscillates with a frequency much higher than the electron gas frequency [69]. Therefore, absorption via classical scattering is much smaller for short

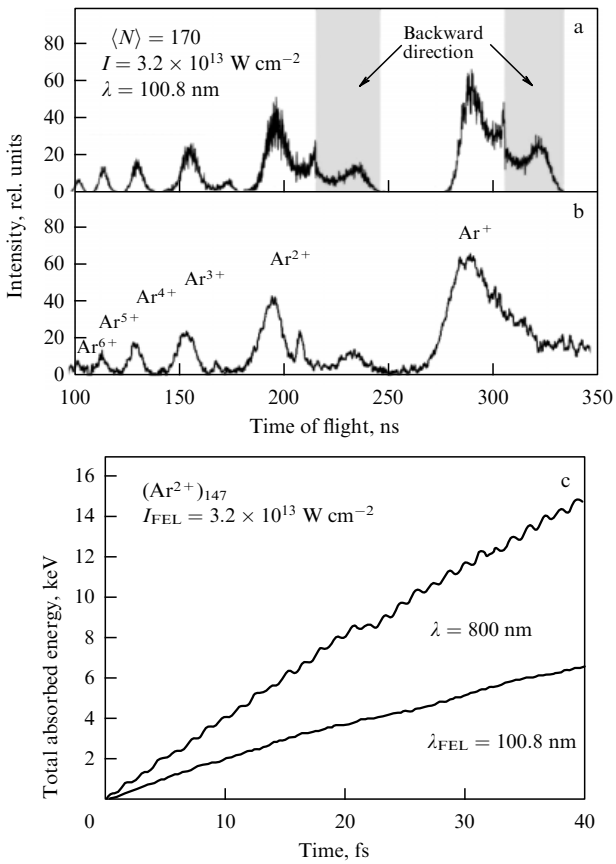

Figure 14. Comparison of theoretical (a) and experimental (b) time-of-flight mass spectra obtained during irradiation of Ar_{170} clusters at a wavelength of 100.8 nm and an intensity of 3.2×10^{13} W cm^{-2}. The spectra also show Ar^+ and Ar^{2+} ions flying out into a hemisphere opposite to the direction toward the detector [132]. (c) Time dependences of calculated energy absorbed by Ar_{147} cluster plasma containing two quasi-free electrons per ion in the laser field at an intensity of 3.2×10^{13} W cm^{-2} for $\lambda = 100.8$ and 800 nm [132].

waves. The plot suggests an almost linear enhancement of the absorbed energy with time at a wavelength of 100.8 nm. The absorption cross section, $\sigma_{\text{sim}} = 5.8$ Mb, derived from the slope of this dependence, is significantly smaller than the experimental one, $\sigma_{\text{exp}} = 24.1$ Mb. It is worth mentioning that the calculated values of the absorption cross section are overestimated because electrons were *a priori* treated as quasi-free and cluster expansion was disregarded. Such a great difference between theory and experiment cannot be interpreted in the context of the standard inverse bremsstrahlung model. It is explained based on the results of recent theoretical studies [74, 137] in which the above-mentioned standard model was further extended. These works will be considered in Section 5.4.

To sum up, the authors of Ref. [132] demonstrated that the specific electronic structure of clusters is practically unrelated to cluster explosion dynamics at laser peak intensities above 1.8×10^{12} W cm^{-2} and acquires significance at a low peak intensity of about 1.9×10^{11} W cm^{-2}. This accounts for the large difference between absorption cross sections of resonant and nonresonant excitations. In either case, internal ionization of atoms is saturated at high intensities, and energy absorption depends mainly on the plasma heating rate. MDM calculations indicate that standard collisional heating of the plasma does not explain such large energy absorption.

5.4 The results of simulations of cluster excitation by VUV pulses

The data on cluster interactions with intense VUV pulses of FELs obtained in works [124, 130, 132, 133] aroused great interest because it is difficult to explain such high-charge states of ions as observed in experiment in the framework of the existing 'standard' models of cluster ionization and heating [124]. Cluster heating in multiphoton processes appears unlikely [112, 124] and heating due to plasma resonances is disproved by experimental findings [132, 133], while macroscopic mechanisms of cluster heating (such as cluster surface absorption [80]) are feasible only when the electron oscillation amplitude is commensurate with the cluster diameter. In the case of cluster interaction with VUV pulses emitted by an FEL, this amplitude is smaller than one Bohr radius (see Table 2).

The most likely explanation of the available results is cluster heating due to inverse bremsstrahlung of valence electrons released after single-photon ionization of the clusters and subsequent atomic ionization with the ejection of internal electrons in collisions between free electrons and ions. However, the rate of this process is too low to account for the observed high-charge states of the clusters. A few mechanisms of effective cluster heating during excitation by VUV pulses have been proposed thus far (see, for example, paper [8] and references cited therein). Among these are, say, an atomic, non-Coulomb contribution to inverse bremsstrahlung [137]; charge-enhanced one-photon ionization [74], and many-body recombination (MBR) [80, 87, 88]. In what follows, we shall briefly consider these mechanisms.

Reference [137] develops a statistical approach, and the cluster is regarded as a bulk plasma heated by VUV radiation. The authors hold to the idea that electrons in a dense cluster plasma are exposed not only to the influence of the conventional Coulomb potential but also to the effects of ion shielding by electrons. In order to account for the high absorbed energy, they introduced a modified Coulomb potential in the form

$$V_Z(R) = -\frac{Z + [Z' - Z]\exp(-\alpha_Z R)}{R} \exp\left(-\frac{R}{\lambda_{\text{D}}}\right), \quad (5.2)$$

where Z is the ion charge, Z' is the nucleus charge, and λ_{D} is the Debye length. Parameter α_Z was introduced to obtain a smooth passage from the potential $-Z/R$ for $\alpha_Z R \gg 1$ to the potential $-Z'/R$ in the case of $R \to 0$. Parameter α_Z was chosen so as to exactly reproduce the first ionization potential of an individual atom.

The system of equations was solved for time-dependent probabilities $n_0(t), n_1(t), \ldots$ for atomic charge states together with the expression for the temporal evolution of electron temperature on the assumption that the plasma heating mechanism is inverse bremsstrahlung. At first, the standard atomic potential was used, then the modified potential (5.2). It was shown in Ref. [137] that this approach results in an approximately one order of magnitude greater number of photons absorbed from the laser pulse field and in excellent agreement between predicted distributions of ion charge states and experimental data obtained in Ref. [124].

According to the authors' opinion, absorption of a large number of photons is due to inverse bremsstrahlung and collisional processes of the (e, 2e) type that occur during the course of the exciting pulse. Absorption of many photons is a multistep event. Each plasma electron is scattered many times

during the course of the pulse, but only one photon is absorbed at each electron–ion collision. Thereafter, the Boltzmann distributions of electrons and ions with common temperatures set in, giving rise to ions with a high charge number.

The substance of charge-enhanced single-photon internal ionization of clusters [74] excited by laser radiation at a wavelength of 100 nm is as follows. The photon energy (12.7 eV) contributing to the excitation of an individual atom is sufficient to induce only single Xe atom ionization. However, the situation changes dramatically when a cluster is excited. Charges of the neighboring atoms in the cluster cause the efficient threshold of internal atomic ionization to lower. In this case, the effective binding energy for internal ionization of cluster atoms is given by

$$E_{\text{eff}} = E_{\text{bar}} - E_{\text{b}}\,, \tag{5.3}$$

where E_{bar} is the energy of the nearest barrier for an atom or an ion to be ionized, and E_{b} is the energy of a bound electron (electron binding energy in an atom plus the potential energy of electron interaction with the laser field and surrounding ions). Under conditions where a photon with a laser field energy $\hbar\omega > |E_{\text{bar}}|$ is absorbed, atomic ionization releases an outer electron; from this instant of time, the electron is regarded as a classical particle. In principle, this process may repeat until ionization of all atoms in the cluster is completed. However, in the majority of the cases Xe atoms undergo ionization mostly through the ejection of 5s- and 5p-electrons (see Section 5.5.3. and Ref. [53]). The mechanism being considered leads to a considerable lowering of the ionization potential of cluster atoms [74], the formation of atomic ions in higher-charge states, and much greater absorption compared with that due to the usual bremsstrahlung effect.

Detailed analysis of the interaction of intense VUV-FEL pulses and near-IR pulses with clusters has recently been reported in Refs [80, 87, 88]. The analysis was made in the context of a dense strongly coupled plasma (SCP). The proposed approach is based on the fact that cluster interaction with intense femtosecond laser pulses gives rise to forming SCP. Such plasma is characterized by a high density of charged particles and frequent multiple electron–electron, electron–ion, and ion–ion collisions. This observation brought the authors to the discovery of a new electron heating mechanism underlain by frequent multiparticle collisions leading to intense recombination of free electrons into excited states undergoing efficacious secondary atomic ionization with the release of these electrons. The authors designated this process as electron heating due to MBR. It is repeated ionization of atoms and ions that is responsible for high radiation absorption by clusters and eventually to their strong heating and formation of ions with a large charge number.

Unlike macroscopic plasma, nanoplasma arising from interactions of intense laser pulses with clusters and containing a finite number of particles can be analyzed by the MDM. It is one type of plasma allowing exact calculations for a large number of particles. Moreover, the results of these calculations reflecting the charge state of the ions, as well as electron and ion energies are amenable to comparison with the available experimental data. This provides a sensitive test for calibrating numerical calculations. Also, the results of such studies form a solid basis for the theoretical description of macroscopic plasma. Analysis of cluster interactions with

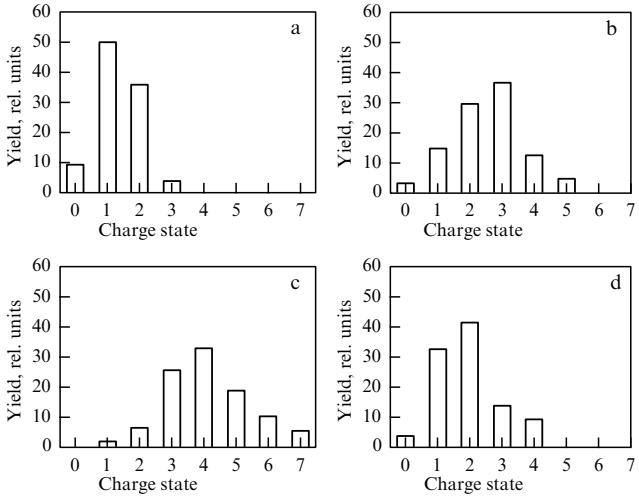

Figure 15. Charge state distribution of ions produced during interaction of Xe clusters with FEL radiation at a wavelength of 98 nm and a pulse length of 100 fs: (a–c) Xe_{1000} at intensities of 1.5×10^{12}, 1.5×10^{13}, and 7×10^{13} W cm^{-2}, respectively, and (d) Xe_{80} at an intensity of 2.0×10^{13} W cm^{-2} [88].

intense laser pulses by the MDM as described in Refs [80, 87, 88] greatly promoted understanding the functional properties of ultrafast electron dynamics in the dense cluster plasma.

Jungreuthmayer and coworkers [87, 88] analyzed interactions between VUV radiation and clusters by the example of an Xe_{1000} cluster slightly smaller in size than Xe_{1500} clusters studied in the FEL experiment [124]. However, other parameters of the model were close to experimental ones, which makes possible qualitative comparison of simulated and observed quantities. The quantitative description is difficult in either case due to uncertainties related to determining cluster size and VUV pulse shape (see Section 4.3).

Figure 15a–d illustrates ion charge distributions for Xe_{1000} clusters exposed to VUV laser radiation at intensities of 1.5×10^{12}, 1.5×10^{13}, and 7×10^{13} W cm^{-2}, and also for Xe_{80} clusters irradiated at the intensity of 2×10^{13} W cm^{-2}. In all calculations, the radiation wavelength was $\lambda = 98$ nm, and the half-height pulse length 100 fs. Ion charge states were determined at an instant of time corresponding to the pulse end, when free electrons were leaving the cluster. A fairly good agreement between theory and experiment was obtained [124] (see Figs 8 and 15). Charge states of up to Xe^{3+} and Xe^{5+} formed at radiation intensities 1.5×10^{12} and 1.5×10^{13} W cm^{-2}, respectively (Fig. 15a, b), were in excellent agreement with experiments on cluster excitation by FEL pulses. At an intensity of 7×10^{13} W cm^{-2}, ions of up to Xe^{7+} were examined (only one charge state lower than in experiment). In the general case, calculated ion charge distribution functions have maxima somewhat shifted toward higher charges than in experiment. The difference is due to the fact that laser beam intensity was not averaged over the cross section for the purpose of calculations [87, 88]. Taking into account the transverse distribution of beam intensity for Xe_{80} clusters was shown [88] to further improve agreement between theory and experiment.

The data presented in Fig. 16 demonstrate that the MBR of electrons into bound states and subsequent secondary atomic ionization are the main factors determining electron dynamics in a dense strongly bound cluster plasma. The

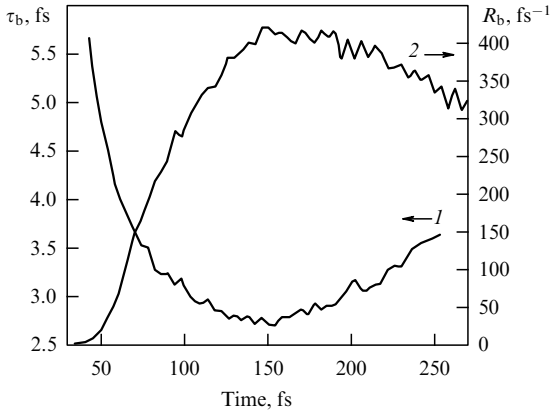

Figure 16. Lifetime τ_b (referred to the $1/e$ level) of the many-body recombination of bound electrons (curve *1*) and MBR rate R_b (number of electrons undergoing recombination into bound states for 1 fs) (curve *2*) depending on time [88].

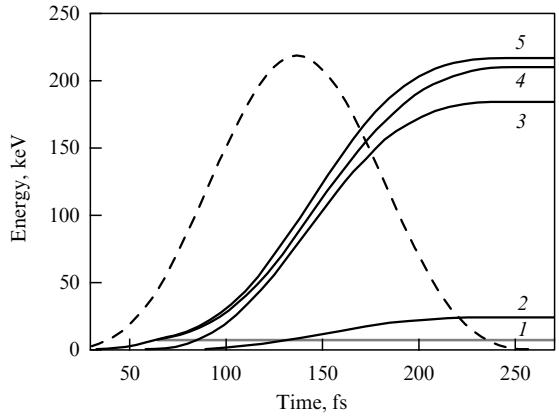

Figure 18. Absorbed energy as a function of time for different mechanisms of Xe_{1000} cluster heating at an intensity of 7×10^{13} W cm^{-2} (as in Fig. 15c): *1* — single-photon absorption, *2* — inverse bremsstrahlung, *3* — MBR-assisted absorption, *5* — total absorption shown by curves *1–3*, *4* — total absorbed energy computed by the MDM. Dashed line — FEL pulse shape [88].

authors of Refs [87, 88] calculated the lifetime τ_b (referred to the $1/e$ level) and the rate R_b of the many-body recombination given by the rate equation

$$\frac{dn_b}{dt} = -\frac{n_b}{\tau_b} + R_b(t)\,. \tag{5.4}$$

Here, n_b is the number of electrons bound due to MBR, and R_b is a function of the temperature and number density of free electrons. As follows from Fig. 16 (curve *1*), the lifetime of bound electrons is on the order of several femtoseconds. It decreases at the onset of a laser pulse, lowers to a minimum at the pulse maximum, and thereafter slowly increases at the pulse trailing edge.

Calculations [87, 88] showed that the energy absorbed in dense plasma via inverse bremsstrahlung is considerably (about one order of magnitude) higher than the absorbed energy in standard inverse bremsstrahlung theories [144]. The main factor responsible for the enhanced efficiency of dense plasma heating through inverse bremsstrahlung is the new heating mechanism, namely, many-body recombination (Fig. 17). Many-particle collisions result in efficacious recombination of electrons into excited bound states (Fig. 17a, b). The remaining free electrons absorb energy during the transition of one of them into an excited bound state (Fig. 17b). Further collisions lead either to repeated atomic ionization with the release of a recombined electron or to electron scattering from the highly excited state into lower states. In this way, a wide range of excited states are populated. The MBR heating cycle is completed when the recombined electron undergoes secondary excitation or when the atom is ionized by an absorbed photon (Fig. 17c). Because recombined electrons continuously orbit the ion, radiation is absorbed more efficiently than in cluster heating through the usual inverse bremsstrahlung, when an electron absorbs radiation only after it encounters the ion. The soundness of this line of reasoning is confirmed by the quantitative data presented below.

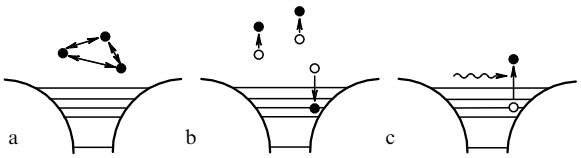

Figure 17. Schematic of cluster heating due to MBR realized in a three-process cycle. Collisions of two or more electrons near an ion (a) lead to MBR into a highly excited bound state (b). Further collisions scatter electrons into deeper bound states and thereby populate a wide spectral range of excited states. The total energy of the multielectron ionic system is conserved (b). The energy is absorbed due to secondary atomic ionization by laser radiation with the release of recombined bound electrons (c) [88].

The predominant contribution of MBR to the total energy absorbed by a cluster is demonstrated in Fig. 18 showing the time dependence of the absorbed energy for radiation parameters presented in Fig. 15c. Curve *4* exhibits the simulated total absorbed energy. Curve *1* illustrates absorption due to single-photon ionization, and curve *2* corresponds to cluster plasma heating via inverse bremsstrahlung calculated in the framework of the standard theory [90, 145]. Curve *3* characterizes energy absorbed by electrons recombined into excited states. This energy is roughly one order of magnitude higher than that necessary for primary single-photon ionization and heating of a cluster through conventional inverse bremsstrahlung. Taken together, these observations confirm that MBR is a major factor underlying the mechanism of cluster plasma heating. Curve *5* illustrates the total absorbed energy (summarized energy, curves *1–3*). The fairly good agreement between curves *4* and *5* indicates that the total absorbed energy is actually a function of the three heating mechanisms (curves *1–3*).

To conclude this section, it is worth mentioning Ref. [138], where interactions between a small Xe_{54} cluster and short laser pulses at 800 and 100 nm were studied in the context of a microscopic approach. In both cases, shock ionization was insignificant. The dominant mechanism was ionization by a quasistatic radial electric field (ignition mechanism; see Section 3.5) created by cluster external ionization. Cluster heating and external ionization depended on the radiation wavelength. Energy absorption at a wavelength of 800 nm, when the electron oscillation amplitude was comparable with the cluster size, mostly occurred in collisions between electrons and the cluster boundary region. At 100 nm, absorption due to inverse bremsstrahlung prevailed.

5.5 Other FEL applications

The FEL at Hamburg was utilized in many other experiments, e.g., to study the multiphoton ionization of atoms and molecules in the gas phase [51 – 53, 112], the photoelectric effect at ultrahigh radiation intensities [53], the photoablation of materials [113], and the two-photon ionization of rare gas atoms in a beam [114]. In what follows (Sections 5.5.1 – 5.5.3), we shall consider in brief these FEL experiments.

5.5.1 Multiphoton ionization of atoms and molecules. The photoionization in the VUV region is usually used for the study of the many-electron dynamics of free atoms and molecules [146]. Until recently, synchrotron radiation has been used for this purpose, alternative sources being unavailable. However, at the levels of power achieved with the help of synchrotron radiation, all processes exhibit linear behavior as radiation intensity grows. Possibilities for the investigation of ultrafast nonlinear effects inherent in interactions between a high-intensity electromagnetic field and matter were extended by recent progress in the generation of intense VUV-FEL radiation [49 – 53] and higher harmonics [147 – 149]. Researchers were enabled to move from studies in the visible region [150] to experiments within the spectral range where the energy of a radiation quantum exceeds the ionization threshold of atoms and molecules.

The authors of Ref. [112] investigated multiphoton ionization of Ar and Xe atoms in an atomic beam by time-of-flight spectrometry. The atoms were exposed to intense FEL pulses at a wavelength of 98 nm (photon energy ca. 12.7 eV), pulse length of around 100 fs, and radiation intensity up to 10^{13} W cm^{-2}. The mass spectra of the ions being formed were measured. Photon energy at the above wavelength was sufficient to induce single-photon ionization of Xe atoms (ca. 12.13 eV [125]) but remained lower than the first ionization potential of Ar atoms (15.76 eV) and ionization potential of Xe^+ ions (21.2 eV). This means that as many as two FEL photons need to be absorbed when ionizing neutral Ar atoms and Xe^+ ions.

In an experiment at an intensity approaching 10^{13} W cm^{-2}, multiply charged xenon and argon ions (up to Xe^{6+} and Ar^{4+}, respectively) were detected. Based on the dependence of the ion yield on laser radiation intensity, the authors postulated mechanisms for the multiphoton ionization processes. They argue that ionization at the intensities of order $10^{12} - 10^{13}$ W cm^{-2} may be described as a sequence of multiphoton processes. It was found that the yield of multiply charged ions saturates at intensities 5 and 30 times lower than in the case of ionization of the same atoms by radiation pulses at 193 nm [151] and 564 nm [152], respectively. Thus, the results of these experiments confirm the theoretically predicted [153] decrease in saturation intensities of the ion yield with increasing laser radiation frequencies.

Many-photon double ionization of molecular nitrogen (N_2) was investigated in Ref. [51]. FEL pulses 25 fs in length with up to 10^{12} photons each and a photon energy of 38 eV ($\lambda = 32.6$ nm) emitted with a repetition rate of 1 MHz were focused onto a spot having a diameter of 26 μm. The corresponding values of photon number density ($\geqslant 10^{17}$ photons cm^{-2}) and radiation intensity ($\geqslant 2 \times 10^{13}$ W cm^{-2}) are the maximum ones achieved thus far in the soft X-ray spectral region. The nitrogen molecule with its simple diatomic structure was chosen because nitrogen undergoes nonlinear two-photon ionization at a photon energy of 38 eV, the first and the second ionization potentials being 15.6 and 23.3 eV, respectively [125]. The authors of Ref. [51] observed multiphoton double ionization of nitrogen molecules, in which the first absorbed photon induced single ionization of the molecule, and the second one ionized the resultant ion. It was concluded that successive multiphoton ionization is more efficient than the direct multiphoton process. Moreover, the sequential process can even be regarded as a direct one enhanced by resonance and proceeding via a real rather than a virtual level. It is worthy of note, however, that interpretation of multiphoton ionization of atoms and molecules by VUV radiation is still in its infancy.

The photoeffect in the extreme UV region was recently exposed in Ref. [53] using powerful FEL pulses. Photoionization of Xe atoms was observed at a wavelength of 13.3 nm ($\hbar\omega \approx 93$ eV) and ultrahigh intensities achieved with an FEL. The experiments were carried out within an exciting radiation intensity range from approximately 10^{12} to 10^{16} W cm^{-2}. Laser pulses were 10 ± 2 fs in length [154]. A time-of-flight mass spectrometer was used to detect ions in charge states of up to Xe^{21+}, which is significantly higher than the charge states observed during Xe ionization at a wavelength of 800 nm (Xe^{8+}) and the same intensity (10^{16} W cm^{-2}) [155]. Almost 5 keV of energy per atom (or more than 57 photons with an energy of 93 eV) had to be absorbed from the laser field during a 10-fs pulse to ensure the formation of Xe^{21+} ions. The dependences of charge states on radiation intensity were examined. The ponderomotive energy of electrons in a laser field being considerably smaller (a few orders of magnitude) than the radiation quantum energy, approaches to the description of the cluster–radiation interaction in the visible region are unsuitable for the range examined in the experiments under consideration. An adequate theoretical basis for the description of the interaction of extreme UV radiation with matter at high intensities remains to be developed.

An FEL was utilized to evaluate the probability of one-, two-, three-, and four-photon ionization processes for neon and helium atoms. The atoms were excited by 25-fs pulses emitted with a repetition rate of 5 kHz and an intensity of up to 10^{14} W cm^{-2}. In order to elucidate ionization mechanisms and compare different successive and multiphoton excitation schemes, the experiments were carried out at two photon energies, 42.8 and 38.4 eV. These energies were slightly higher and lower than the threshold for successive two-photon double ionization of Ne atoms via Ne^+ ions at an energy of 41.0 eV, the first and the second ionization potentials being 21.56 and 40.96 eV, respectively [125]. These two cases may be substantially different in terms of the character of nonlinear dependences of ion yield on laser radiation intensity. Experiments [52] allowed cross sections of two-photon ionization of neon and helium atoms and Ne^+ and Ne^{2+} ions to be determined and showed the dominant role of sequential multiphoton transitions via ionic and resonant states, as opposed to direct multiphoton transitions through virtual states.

5.5.2 Ablation of materials. An interesting application of an FEL emitting in the VUV range is described in Ref. [113], which investigated the ablation of an organic polymer (polymethylmethacrylate plus silicon) film by single extreme UV pulses generated from a Z-pinch plasma focus or a laser plasma. Ablation characteristics obtained with the help of plasma sources of radiation were compared with those

obtained during irradiation of the same samples by UV pulses from an FEL.

The exposure of organic polymers to intense extreme UV radiation in a vacuum results in the transfer of macroscopic amounts of the irradiated material to the vacuum. Sources of low-intensity radiation remove the material through its photon-induced desorption from the irradiated surface (dry etching or evaporation by synchrotron radiation). Each photon of extreme UV radiation is able to break any chemical bond. The photon energy is normally greater than the atom binding energy in a crystal. High-energy photons of extreme UV radiation excite electrons from inner electron shells. This process is followed by a cascade of Auger transitions leading to the formation of electron-depleted regions that rapidly break down in the course of a Coulomb explosion. Photons absorbed near the surface may cause sample disintegration into small fragments ejected into the vacuum. Low-intensity radiation withdraws material only from the surface and subsurface layers of the sample.

The situation is quite different when single pulses of high-energy radiation are utilized. In this case, a large local radiation dose enters a sample at a high rate. Therefore, a large number of elementary acts responsible for structural changes in the material occur almost simultaneously in a relatively thick layer exposed to radiation, provided its absorption of radiation is not too high. Most of the absorbed energy undergoes thermalization, rapidly overheats the irradiated layer, and alters the chemical composition of the layer. The overheated fragmented part of the sample makes up a new phase passing into the vacuum. Eventually, ultrashort high-intensity FEL pulses may cause rapid disintegration of the irradiated solid by transferring a large number of electrons from the valence zone to the conduction zone.

Polymethylmethacrylate/silicon samples were irradiated from an FEL at a wavelength of 86 nm ($\hbar\omega \approx 14.3$ eV) by pulses < 100 fs in duration at an intensity of about 10^{12} W cm^{-2}. It was shown in Ref. [113] that exposure of polymethylmethacrylate (PPMA) to UV radiation from plasma sources leads to the strong heating of the sample and causes marked morphological changes to irradiated surface. The material is decomposed with the formation of a black carbon (soot) deposit and blisters at its surface. At the same time, the surface of PMMA samples exposed to FEL pulses remains moderately even, with its structure and composition being practically unaltered (Fig. 19). The depth of the spot (ca. 25 μm) at the surface left by a laser pulse train and measured by optical spectroscopy suggests that a single pulse knocks out approximately 70 nm of the material from the surface. The FEL radiation attenuation length in PMMA being about 10 nm [156], it can be concluded that PPMA ablation occurs at an intensity roughly three orders of magnitude lower than used in experiment. Thus, the above studies provided very promising results to be used for the microprocessing of miniature components and surfaces by short-wave VUV radiation from an FEL.

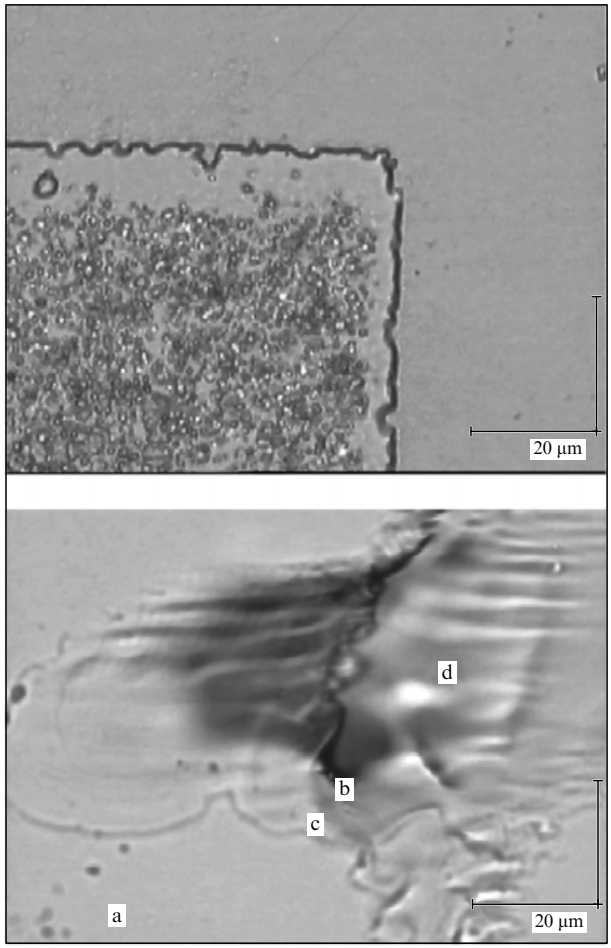

Figure 19. The surface of a PMMA film sample after exposure to extreme UV radiation pulses. Top: irradiation by a nanosecond pulse of Cu-plasma. The sample is placed behind a mesh contact at 50 cm from the source. Bottom: irradiation by FEL pulses at 86 nm. The crater formed after the irradiation of the film by 380 pulses < 100 fs in length with an energy of 5 μJ at an angle of incidence of 55°. Film composition after irradiation was analyzed at points a–d by Raman spectra [113].

5.5.3 Two-frequency two-photon ionization of Xe atoms. This section deals with FEL applications in combination with other lasers. The recent work [114] describes a unique experimental setup for the study of interactions of an FEL radiation with matter. It comprises an FEL operating in the extreme UV region ($\lambda = 13.7$ nm) and producing pulses of length $\tau_p = 10-50$ fs, a laser generating high-power ultra-short IR pulses ($\lambda = 800$ nm, $\tau_p = 110$ fs), and a picosecond laser emitting in the visible range ($\lambda = 523$ nm, $\tau_p = 12$ ps). The combination of an FEL with a synchronized infrared laser or a visible laser opens up considerable opportunities for experimenting on two-frequency excitation–probing of atoms and molecules in the gaseous phase, clusters, plasma, and condensed media. It has already brought about the first data on two-frequency two-photon ionization of rare gas atoms with high time resolution. We shall briefly consider this method and the results obtained with its help.

The excitation–probing method for the analysis of a photoelectron signal induced by FEL photons in the presence of powerful visible or near-IR laser radiation requires photoelectron spectroscopy [114, 157]. The best method for measuring the delay time between two pulses over a time scale comparable to FEL and optical laser pulse lengths (in the femtosecond range) is two-frequency above-barrier (tunnel) ionization. When extreme UV and near-IR pulses overlap in space and time, photoelectrons generated by UV pulses occur in the field of a probing pulse from the optical laser, where they can absorb one or several photons emitted by this laser. This leads to the appearance of side bands (SBs) in the corresponding photoelectron spectrum of a target atom

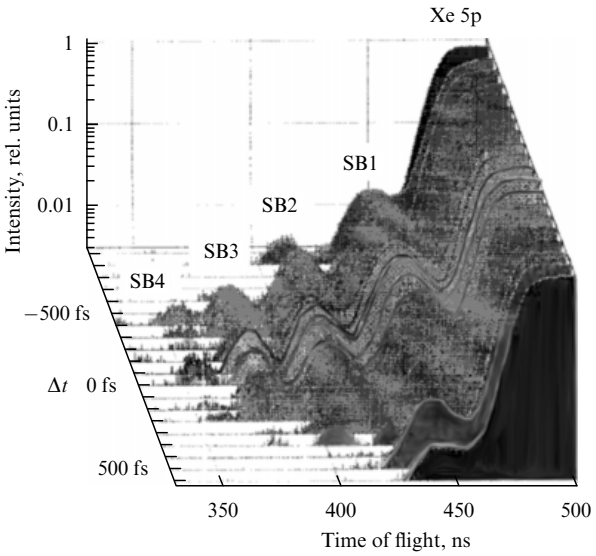

Figure 20. Time-of-flight spectra taken in two-frequency two-photon ionization of xenon atoms by extreme UV-FEL and optical laser radiation. Different spectra are represented as a function of delay time between FEL pulses ($\lambda = 13.8$ nm, $\tau_p = 20$ fs) and optical pulses ($\lambda = 800$ nm, $\tau_p = 120$ fs, energy 20 μJ) [114].

[158, 159]. Their shape and intensity strongly depend on temporal and spatial profiles of two femtosecond pulses [160]; therefore, these parameters can be used to elucidate FEL pulse characteristics [158, 161) and to measure directly a delay time between two laser pulses [159]. Changes in the delay time are effected using a computer-controlled optical delay line. The synchronization of two pulses of different frequencies in the excitation–probing scheme was demonstrated for xenon atoms as a target gas.

Under experimental conditions, laser pulses were focused onto the zone of their intersection with a beam of xenon atoms. The yield of electrons induced by two-frequency ionization of Xe atoms was measured, along with the accompanying release of 5p electrons at an FEL wavelength of 13.7 nm ($\hbar\omega = 89.9$ eV) (Fig. 20). Each time-of-flight mass spectrum displayed in Fig. 20 was averaged over 250 pulses of both lasers. The intense field of the near-IR laser gives rise to rather intense SBs (SB1–SB4, see Fig. 20) formed due to the absorption of up to 4 optical photons. It can be seen that SBs occur only within a time interval of about 600 fs. The width of temporal pulse overlap (ca. 600 fs) deduced from SB formation in the spectrum is largely determined by a spread in time of FEL pulses with respect to an optical pulse. The band width gives a time resolution of about 250 fs [159]. It can be greatly improved (up to 50 fs) due to the possibility of detecting the spectrum within a single laser shot [114]. The delay time between the pulses is measured in each shot. Thus, the experimental setup of interest and the measuring method used allow for studying interactions of FEL pulses of extreme UV radiation with matter with a high time resolution (on the order of 50 fs). The potential possibilities of applying an FEL operated in the X-ray range to the exploration of matter with high temporal and spatial resolution in excitation–probing experiments were considered in Ref. [115].

To conclude this section, it should be emphasized that new considerable opportunities for applying VUV-FEL radiation in many basic and applied research fields have raised great interest in the construction of such lasers as light sources of the fourth generation [104 – 108]. As many as 15 projects for the development of FELs operating in the VUV and X-ray ranges are currently underway [104] in the USA [104, 162 – 164], Germany [104, 165 – 171], Japan [104, 172 – 175], Italy [104, 176 –178], France [104, 179], the UK [104, 180], and South Korea [104, 181]. The projects being implemented at Stanford (USA) and Hamburg (Germany) are expected to produce FEL X-ray emission with a wavelength of 1 – 1.5 Å in the near future (by 2010 – 2012) [104].

6. Conclusions

With the advent of FELs operating in the VUV range, the parameters of interaction of radiation with matter, in particular, atomic cluster beams, were substantially extended, making it possible to study the character of cluster interaction with the laser field under conditions formerly unrealizable. The results of these studies indicate that a change in the exciting radiation wavelength has a dramatic effect on the reciprocal behavior of collective and collisional processes in dense cluster plasma. New mechanisms of rare gas cluster interaction with VUV-FEL radiation have been proposed, including accurate consideration of the effects of atomic potential [137], charge-enhanced ionization [74], collisional heating [124, 130], and many-particle collisions and recombination [87, 88]. Many of these mechanisms much more effectively heat dense cluster plasma than conventional stimulated inverse bremsstrahlung.

The results of the studies do not allow for a unified simple description of absorption of intense laser pulses by clusters. They suggest a variety of mechanisms and processes behind cluster excitation by superhigh-power ultrashort laser pulses depending not only on the characteristics of the exciting radiation but also on the cluster size and the time of cluster plasma evolution. Some of these mechanisms and processes become predominant under certain conditions. At the same time, it should be noted that the evolution of cluster plasma begins from ionization of cluster atoms and ions by a strong electromagnetic wave, as a fastest process of primary formation of free electrons. This creates conditions for the subsequent development of cluster plasma via different channels. In the case of cluster excitation by VUV-FEL radiation, primary free electrons are produced in the course of direct and successive one-photon and multiphoton ionization of cluster atoms and ions. When clusters are excited by IR and visible light radiation, free electrons are formed via above-barrier (tunnel) ionization of cluster atoms and ions in the field of a strong electromagnetic wave.

The available data on cluster interaction with intense ultrashort laser pulses suggest the existence of different mechanisms of pulse energy absorption and cluster plasma heating. The principal absorption mechanism for cluster excitation at 800 nm is resonant absorption. It applies to almost all optically active electrons in the cluster and therefore predominates over other mechanisms that enter into operation only when resonant absorption is for some reason infeasible. Cluster excitation by VUV radiation at a wavelength of 100 nm creates quite a different situation in which the most efficient energy absorption mechanisms are inverse bremsstrahlung, MBR, and probably some others. Further experiments are needed to clarify the causes of such high absorption.

The studies carried out thus far have shown that certain concepts known from the physics of cluster interaction with

intense low-frequency radiation pulses are applicable to cluster excitation by high-energy photons. However, a deeper insight into the underlying processes and a more detailed description of the atomic behavior in the plasma formed are needed to realize their application. By way of example, cluster excitation by intense pulses of even shorter-wavelength (X-ray) radiation ($\lambda \approx 3-5$ nm, $\hbar\omega \approx 250-400$ eV) may lead to complete ionization of atomic clusters and a huge Coulomb explosion of the clusters because ionization of clusters interacting with X-ray radiation proceeds in a fundamentally different way than in the case of optical pumping [182]. Ionization starts from inner electron shells of cluster atoms since its cross section in the case of X-ray excitation is greater for inner than for outer valence shells [145]. Typical values of inverse ionization rate are $1-10$ fs [182], or much smaller than the laser pulse length. Hence the possibility of multiple single-photon ionization of cluster atoms owing to the fact that inner atomic shells emptied by the laser pulse are filled up through Auger transitions. Auger relaxation is practically independent of the atomic charge state and takes very little time ($0.2-5$ fs) [183]. Due to such practically instantaneous population of inner atomic shells by electrons, they can undergo multiple one-photon ionization during the passage of an exciting laser pulse, in a clear contrary to the mechanism of atomic ionization by optical pulses, where electrons are primarily removed from outer atomic shells.

The results of experimental and theoretical studies shed light on the nature of atomic cluster interactions with intense femtosecond VUV laser pulses. Interactions of high-energy photons with clusters in this new regime give rise to many interesting and surprising phenomena. The creation of an FEL operating in the VUV and X-ray ranges will stimulate further cluster experiments of importance for studying and understanding radiation–matter interaction. There is reason to expect new interesting and important data in the nearest future that will expose new interaction mechanisms and extend the knowledge of the physical mechanisms underlying excitation of cluster matter. This, in turn, will promote more deep understanding of the processes of radiation–matter interaction and wider application of cluster beams in basic and applied research. To mention but one essential example, it may improve the accuracy of estimating the matter disintegration threshold and permit obtaining images with high (angström-level) temporal and spatial resolution, which is of special importance for biological applications of the lasers considered in this review.

To conclude, the development of FELs emitting in the VUV and soft X-ray ranges and investigations into interactions of radiation and matter with the use of these devices are expected to contribute first and foremost to fundamental research. The results thus obtained will find practical application only after a lapse of time. At present, the immediate task is to accumulate new data and develop appropriate methods for their practical use. It is clear that this field of physics is of paramount importance for many practical purposes. Some results of the studies may prove to be of great practical value in the short run in such disciplines as nanotechnology, materials science, biology, and medicine. This area of research and development characterizes the current state and progress of high technologies in many advanced countries. FELs emitting in the VUV and X-ray ranges are being developed and constructed in the USA, Germany, Japan, France, Italy, and Great Britain. Unfortunately, there are no such lasers in Russia, nor can relevant research be carried out as the result of dramatic underfinancing of science. It may eventually lead to the widening of Russia's technology gap with other industrialized nations in many important areas of science and technology development.

The author is grateful to E A Nikolaeva for her assistance in literature searches, and to A N Petin for assistance in the preparation of the drawings. The valuable comments of the reviewer are acknowledged. The work was supported in part by the Russian Foundation for Basic Research (grants Nos 06-02-16634, 07-02-00165, and 09-02-00531).

References

1. Ditmire T et al. *Phys. Rev. A* **53** 3379 (1996)
2. Ditmire T et al. *Phys. Rev. A* **57** 369 (1998)
3. Krainov V P, Smirnov M B *Usp. Fiz. Nauk* **170** 969 (2000) [*Phys. Usp.* **43** 901 (2000)]
4. Krainov V P, Smirnov M B *Phys. Rep.* **370** 237 (2002)
5. Zweiback J et al. *Phys. Plasmas* **9** 3108 (2002)
6. Smirnov B M *Usp. Fiz. Nauk* **173** 609 (2003) [*Phys. Usp.* **46** 589 (2003)]
7. Smirnov M B, Krainov V P *Phys. Rev. A* **69** 043201 (2004)
8. Saalmann U, Siedschlag Ch, Rost J M *J. Phys. B* **39** R39 (2006)
9. Krainov V P, Smirnov B M, Smirnov M B *Usp. Fiz. Nauk* **177** 953 (2007) [*Phys. Usp.* **50** 907 (2007)]
10. Makarov G N *Usp. Fiz. Nauk* **176** 121 (2006) [*Phys. Usp.* **49** 117 (2006)]
11. Makarov G N *Usp. Fiz. Nauk* **178** 337 (2008) [*Phys. Usp.* **51** 319 (2008)]
12. Ditmire T et al. *Nature* **386** 54 (1997)
13. Last I, Jortner J *Phys. Rev. A* **73** 013202 (2006)
14. Springate E et al. *Phys. Rev. A* **61** 044101 (2000)
15. Auguste T et al. *J. Quantit. Spectrosc. Rad. Transf.* **71** 147 (2001)
16. Skobelev I Yu et al. *Zh. Eksp. Teor. Fiz.* **121** 88 (2002) [*JETP* **94** 73 (2002)]
17. Maltsev A, Ditmire T *Phys. Rev. Lett.* **90** 053002 (2003)
18. Parra E et al. *J. Opt. Soc. Am. B* **20** 118 (2003)
19. McPherson A et al. *Nature* **370** 631 (1994)
20. Dobosz S et al. *Phys. Rev. A* **56** R2526 (1997)
21. Ditmire T et al. *Appl. Phys. Lett.* **71** 166 (1997)
22. Stenz C et al. *Kvantovaya Elektron.* **30** 721 (2000) [*Quantum Electron.* **30** 721 (2000)]
23. Junkel-Vives G C et al. *J. Quantit. Spectrosc. Rad. Transf.* **71** 417 (2001)
24. Skobelev I Yu et al. *Zh. Eksp. Teor. Fiz.* **121** 1124 (2002) [*JETP* **94** 966 (2002)]
25. Magunov A I et al. *Laser Part. Beams* **21** 73 (2003)
26. Fukuda Y et al. *Pis'ma Zh. Eksp. Teor. Fiz.* **78** 146 (2003) [*JETP Lett.* **78** 115 (2003)]
27. Abdallah J (Jr.) et al. *Phys. Rev. A* **68** 063201 (2003)
28. Fukuda Y et al. *Laser Part. Beams* **22** 215 (2004)
29. Ivanova E P, Ivanov A L *Zh. Eksp. Teor. Fiz.* **127** 957 (2005) [*JETP* **100** 844 (2005)]
30. Kim K Y et al. *Phys. Rev. E* **73** 066403 (2006)
31. Smirnov M B, Becker W *Phys. Rev. A* **74** 013201 (2006)
32. Ditmire T et al. *Nature* **398** 489 (1999)
33. Zweiback J et al. *Phys. Rev. Lett.* **84** 2634 (2000)
34. Zweiback J et al. *Phys. Rev. Lett.* **85** 3640 (2000)
35. Last I, Jortner J *J. Phys. Chem. A* **106** 10877 (2002)
36. Madison K W et al. *J. Opt. Soc. Am. B* **20** 113 (2003)
37. Madison K W et al. *Phys. Plasmas* **11** 270 (2004)
38. Madison K W et al. *Phys. Rev. A* **70** 053201 (2004)
39. Buersgens F et al. *Phys. Rev. E* **74** 016403 (2006)
40. Grillion G et al. *Phys. Rev. Lett.* **89** 165005 (2002)
41. Ter-Avetisyan S et al. *Phys. Rev. Lett.* **96** 145006 (2006)
42. Krainov V P, Smirnov B M *Zh. Eksp. Teor. Fiz.* **132** 634 (2007) [*JETP* **105** 559 (2007)]
43. McPherson A et al. *Phys. Rev. Lett.* **72** 1810 (1994)
44. Schroeder W A et al. *J. Phys. B* **31** 5031 (1998)

45. Arthur J et al. (The LCLS Design Study Group), Linac Coherent Light Source (LCLS) Design Study Report, SLAC-R-521 (Stanford, Calif.: Stanford Univ., 1998)
46. Arthur J *Rev. Sci. Instrum.* **73** 1393 (2002)
47. Richard F et al. (Eds),TESLA Technical Design Report, DESY 2001-011, Pt. I (Hamburg: DESY, 2001)
48. Materlik G, Tschentscher T (Eds) "The X-ray free electron laser", TESLA Technical Design Report, DESY 2001-011, Pt. V (Hamburg: DESY, 2001)
49. Andruszkow J et al. *Phys. Rev. Lett.* **85** 3825 (2000)
50. Ayvazyan V et al. *Eur. Phys. J. D* **37** 297 (2006)
51. Sorokin A A et al. *J. Phys. B* **39** L299 (2006)
52. Sorokin A A et al. *Phys. Rev. A* **75** 051402(R) (2007)
53. Sorokin A A et al. *Phys. Rev. Lett.* **99** 213002 (2007)
54. Keldysh L V *Zh. Eksp. Teor. Fiz.* **47** 1945 (1964) [*Sov. Phys. JETP* **21** 1135 (1965)]
55. Ammosov M V, Delone N B, Krainov V P *Zh. Eksp. Teor. Fiz.* **91** 2008 (1986) [*Sov. Phys. JETP* **64** 1191 (1986)]
56. Glover T E et al. *Phys. Rev. Lett.* **73** 78 (1994)
57. Rae S C, Burnett K *Phys. Rev. A* **46** 2077 (1992)
58. Kruer W L *The Physics of Laser Plasma Interactions* (Redwood City, Calif.: Addison-Wesley, 1988)
59. Blyth W J et al. *Phys. Rev. Lett.* **74** 554 (1995)
60. Crane J K et al. *J. Opt. Soc. Am. B* **13** 89 (1996)
61. Bethe H A, Salpeter E E *Quantum Mechanics of One- and Two-Electron Atoms* (Berlin: Springer, 1957) [Translated into Russian (Moscow: Fizmatgiz, 1960)]
62. Lotz W *Z. Phys.* **216** 241 (1968)
63. Jackson J D *Classical Electrodynamics* 2nd ed. (New York: Wiley, 1975) [Translated into Russian (Moscow: Mir, 1965)]
64. Ashcroft N W, Mermin N D *Solid State Physics* (New York: Holt, Rinehart and Winston, 1976) [Translated into Russian (Moscow: Mir, 1979)]
65. Kreibig U, Vollmer M *Optical Properties of Metal Clusters* (Berlin: Springer, 1995)
66. Milchberg H M, McNaught S J, Parra E *Phys. Rev. E* **64** 056402 (2001)
67. Last I, Jortner J *Phys. Rev. A* **64** 063201 (2001)
68. Ditmire T *Phys. Rev. A* **57** R4094 (1998)
69. Last I, Jortner J *Phys. Rev. A* **60** 2215 (1999)
70. Last I, Jortner J *Phys. Rev. A* **62** 013201 (2000)
71. Ishikawa K, Blenski T *Phys. Rev. A* **62** 063204 (2000)
72. Toma E S, Muller H G *Phys. Rev. A* **66** 013204 (2002)
73. Siedschlag Ch, Rost J M *Phys. Rev. Lett.* **89** 173401 (2002)
74. Siedschlag Ch, Rost J-M *Phys. Rev. Lett.* **93** 043402 (2004)
75. Saalmann U, Rost J-M *Phys. Rev. Lett.* **91** 223401 (2003)
76. Jurek Z, Faigel G, Tegze M *Eur. Phys. J. D* **29** 217 (2004)
77. Ramunno L et al *J. Phys. B* **39** 4923 (2007)
78. Saalmann U *J. Mod. Opt.* **53** 173 (2006)
79. Saalmann U, Rost J M *Eur. Phys. J. D* **36** 159 (2005)
80. Jungreuthmayer C et al. *Phys. Rev. Lett.* **92** 133401 (2004)
81. Deiss C, Rohringer N, Burgdörfer J *Nucl. Instrum. Meth. Phys. Res. B* **235** 210 (2005)
82. Fomichev S V et al. *J. Phys. B* **36** 3817 (2003)
83. Fomichev S V et al. *Phys. Rev. A* **71** 013201 (2005)
84. Popruzhenko S V, Zaretsky D F, Becker W *J. Phys. B* **39** 4933 (2006)
85. Taguchi T, Antonsen T M (Jr.), Milchberg H M *Phys. Rev. Lett.* **92** 205003 (2004)
86. Kostyukov I Yu *Pis'ma Zh. Eksp. Teor. Fiz.* **73** 438 (2001) [*JETP Lett.* **73** 393 (2001)]
87. Jungreuthmayer C et al. *J. Phys. B* **38** 3029 (2005)
88. Ramunno L, Jungreuthmayer C, Brabec T *Laser Phys.* **17** 618 (2007)
89. Last I, Jortner J *J. Phys. Chem. A* **102** 9655 (1998)
90. Krainov V P *J. Phys. B* **33** 1585 (2000)
91. Rose-Petruck C et al. *Phys. Rev. A* **55** 1182 (1997)
92. Neumann W *The Mechanism of the Thermoemitting Arc Cathode* (Berlin: Akademie-Verlag, 1987)
93. Hoyaux M F *Arc Physics* (New York: Springer-Verlag, 1968)
94. Kostyukov I Yu *Zh. Eksp. Teor. Fiz.* **127** 1026 (2005) [*JETP* **100** 903 (2005)]
95. "A VUV free electron laser at the TESLA Test Facility at DESY", Conceptual Design Report, DESY, TESLA-FEL 95-03 (1995)
96. Brinkmann R et al. (Eds), DESY Report 1997-048 (1997)
97. Brinkmann R et al. (Eds), TESLA XFEL: First stage of the X-ray laser laboratory, Technical Design Report, DESY-2002-167 (2002)
98. Madey J M J *J. Appl. Phys.* **42** 1906 (1971)
99. Kondratenko A M, Saldin E L *Part. Accel.* **10** 207 (1980)
100. Derbenev Ya S, Kondratenko A M, Saldin E L *Nucl. Instrum. Meth. Phys. Res.* **193** 415 (1982)
101. Kim K-J *Phys. Rev. Lett.* **57** 1871 (1986)
102. Krinsky S, Yu L H *Phys. Rev. A* **35** 3406 (1987)
103. Saldin E L, Schneidmiller E A, Yurkov M V *The Physics of Free Electron Lasers* (Berlin: Springer, 2000)
104. Dattoli G, Renieri A *Nucl. Instrum. Meth. Phys. Res. A* **507** 464 (2003)
105. Colson W B *Nucl. Instrum. Meth. Phys. Res. A* **475** 397 (2001)
106. Sonntag B *Nucl. Instrum. Meth. Phys. Res. A* **467** 8 (2001)
107. Couprie M E *C.R. Acad. Sci. IV* **1** 329 (2000)
108. Barletta W, Rizzuto C *Rev. Nuovo Cimento* **29** (6) 1 (2006)
109. Rossbach J (TESLA FEL Study Croup) *Nucl. Instrum. Meth. Phys. Res. A* **375** 269 (1996)
110. Ayvazyan V et al. *Phys. Rev. Lett.* **88** 104802 (2002)
111. Ayvazyan V et al. *Eur. Phys. J. D* **20** 149 (2002)
112. Wabnitz H et al. *Phys. Rev. Lett.* **94** 023001 (2005)
113. Juha L et al. *Nucl. Instrum. Meth. Phys. Res. A* **507** 577 (2003)
114. Radcliffe P et al. *Nucl. Instrum. Meth. Phys. Res. A* **583** 516 (2007)
115. Tschentscher Th *Chem. Phys.* **299** 271 (2004)
116. Rossbach J *Nucl. Instrum. Meth. Phys. Res. A* **475** 13 (2001)
117. Krasilnikov M et al. "Optimizing the PITZ electron source for the VUV-FEL", in *Proc. of EPAC 2004, Lucerne, Switzerland* (2004) p. 360
118. Weise H "Superconducting RF structures — Test facilities and results", in *Proc. of the 2003 Particle Accelerator Conf., Portland, Oregon* Vol. 1 (Piscataway, NJ: IEEE, 2003) p. 673
119. Saldin E L, Schneidmiller E A, Yurkov M V "Expected properties of the radiation from VUV-FEL at DESY (femtosecond mode of operation)", in *Proc. of the 2004 FEL Conf.*, p. 212
120. Pflüger J *Nucl. Instrum. Meth. Phys. Res. A* **445** 366 (2000)
121. Saldin E L, Schneidmiller E A, Yurkov M V *Opt. Commun.* **148** 383 (1998)
122. Saldin E L, Schneidmiller E A, Yurkov M V *Opt. Commun.* **235** 415 (2004)
123. Saldin E L, Schneidmiller E A, Yurkov M V *Opt. Commun.* **281** 1179 (2008)
124. Wabnitz H et al. *Nature* **420** 482 (2002)
125. Lide D R (Ed.) *CRC Handbook of Chemistry and Physics* 74th ed. (Boca Raton: CRC Press, 1993-1994)
126. Rusek M, Lagadec H, Blenski T *Phys. Rev. A* **63** 013203 (2000)
127. Brewczyk M, Rzazewski K *J. Phys. B* **32** L1 (1999)
128. Krainov V P, Roshchupkin A S *J. Phys. B* **34** L297 (2001)
129. Samson J A R *Phys. Lett.* **8** 107 (1964)
130. Schulz J et al. *Nucl. Instrum. Meth. Phys. Res. A* **507** 572 (2003)
131. Augst S et al. *Phys. Rev. Lett.* **63** 2212 (1989)
132. Laarmann T et al. *Phys. Rev. Lett.* **92** 143401 (2004)
133. Laarmann T et al. *Phys. Rev. Lett.* **95** 063402 (2005)
134. de Castro A R B et al. *J. Electron Spectrosc. Relat. Phenom.* **144–147** 3 (2005)
135. Shao Y L et al. *Phys. Rev. Lett.* **77** 3343 (1996)
136. Buck U, Krohne R *J. Chem. Phys.* **105** 5408 (1996)
137. Santra R, Green C H *Phys. Rev. Lett.* **91** 233401 (2003)
138. Bauer D *J. Phys. B* **37** 3085 (2004)
139. Andersen J U, Bonderup E, Hansen K *J. Phys. B* **35** R1 (2002)
140. Riffe D M et al. *J. Opt. Soc. Am. B* **10** 1424 (1993)
141. de Castro A R B et al. *Int. J. Electron Spectrosc. Relat. Phenom.* **156** 25 (2007)
142. Wörmer J et al. *J. Chem. Phys.* **104** 8269 (1996)
143. Brantov A et al. *Phys. Plasmas* **10** 3385 (2003)
144. Pfalzner S, Gibbon P *Phys. Rev. E* **57** 4698 (1998)
145. Amusia M Ya *Atomnyi Fotoeffekt* (Atomic Photoeffect) (Moscow: Nauka, 1987) [Translated into English (New York: Plenum Press, 1990)]
146. Becker U, Shirley D A (Eds) *VUV and Soft X-Ray Photoionization* (New York: Plenum Press, 1996)
147. Miyamoto N et al. *Phys. Rev. Lett.* **93** 083903 (2004)
148. Nabekawa Y et al. *Phys. Rev. Lett.* **94** 043001 (2005)
149. Hasegawa H et al. *Phys. Rev. A* **71** 023407 (2005)

150. Batani D et al. (Eds) *Atoms, Solids, and Plasmas in Super-Intense Laser Fields* (New York: Kluwer Acad./Plenum Publ., 2001)
151. Luk T S et al. *Phys. Rev. Lett.* **51** 110 (1983)
152. Perry M D et al. *Phys. Rev. Lett.* **60** 1270 (1988)
153. Santra R, Greene H *Phys. Rev. A* **70** 053401 (2004)
154. Ackermann W et al. *Nature Photon.* **1** 336 (2007)
155. Yamakawa K et al. *Phys. Rev. Lett.* **92** 123001 (2004)
156. Ferincz I E, Tóth Cs, Young J F *J. Vacuum Sci. Technol. B* **15** 828 (1997)
157. Wellhöfer M et al. *J. Instrum. JINST* **3** 02003 (2008)
158. Meyer M et al. *Phys. Rev. A* **74** 011401(R) (2006)
159. Radcliffe P et al. *Appl. Phys. Lett.* **90** 131108 (2007)
160. Glover T E et al. *Phys. Rev. Lett.* **76** 2468 (1996)
161. Toma E S et al. *Phys. Rev. A* **62** 061801(R) (2000)
162. Arthur J et al. (The LCLS Design Study Group), Report SLAC-R-521 (1998); LCLS Conceptual Design Report for the LCLS Project of the US Department of Energy, SLAC-R-593, UC-414 (2002)
163. Johnson E "VUV-FEL current status and plans", in *TJNAF LPC Workshop, January 2001*
164. Doyuran A et al. *Phys. Rev. Lett.* **86** 5902 (2001)
165. "The TESLA Test Facility FEL Team: SASE FEL at the TESLA Facility, Phase 2", DESY Report TESLA-FEL 2002-01 (2002)
166. Treusch R, Feldhaus J *Eur. Phys. J. D* **26** 119 (2003)
167. Richter M et al. *Appl. Phys. Lett.* **83** 2970 (2003)
168. Dohlus M et al. *Nucl. Instrum. Meth. Phys. Res. A* **530** 217 (2004)
169. Abo-Bakr M et al. *Nucl. Instrum. Meth. Phys. Res. A* **483** 470 (2002)
170. Meseck A et al. *Nucl. Instrum. Meth. Phys. Res. A* **528** 577 (2004)
171. Jaeschke E *Nucl. Instrum. Meth. Phys. Res. A* **543** 85 (2005)
172. Shintake T et al. "Status of SCSS: SPring-8 Compact SASE Source Project", in *EPAC 2002: 8th European Particle Accelerator Conf., Paris, 3 – 7 June 2002*
173. Yamada K et al. *Nucl. Instrum. Meth. Phys. Res. A* **528** 268 (2004)
174. Hosaka M et al. *Nucl. Instrum. Meth. Phys. Res. A* **528** 291 (2004)
175. Hama H et al. *Nucl. Instrum. Meth. Phys. Res. A* **528** 571 (2004)
176. Bocchetta C J et al. *Nucl. Instrum. Meth. Phys. Res. A* **507** 484 (2003)
177. Renieri A *Nucl. Instrum. Meth. Phys. Res. A* **507** 507 (2003)
178. Alesini D et al. *Laser Part. Beams* **22** 341 (2004)
179. Couprie M E et al. *Nucl. Instrum. Meth. Phys. Res. A* **528** 557 (2004)
180. Poole M W, McNeil B W J *Nucl. Instrum. Meth. Phys. Res. A* **507** 489 (2003)
181. Choi J et al. *J. Korean Phys. Soc.* **50** 1372 (2007)
182. Saalmann U, Rost J-M *Phys. Rev. Lett.* **89** 143401 (2002)
183. Kochur A G et al. *J. Phys. B* **28** 387 (1995)